Variations in perfusion detectable in advance of microstructure in white matter aging

Tyler D. Robinson[1], Yutong L. Sun[1], Paul T. H. Chang[1], Claudine J. Gauthier[3*], J. Jean Chen[1,2,4*]

1. Rotman Research Institute, Baycrest, Canada
2. Medical Biophysics, University of Toronto, Canada
3. Physics, Concordia University, Canada
4. Biomedical Engineering, University of Toronto, Canada

Corresponding authors:
J. Jean Chen (jchen@research.baycrest.org)
Tyler D. Robinson (trobinson@research.baycrest.org)
Rotman Research Institute, Baycrest
3560 Bathurst Street
Toronto ON, Canada M6A 2E1

*co-senior authors

Acknowledgments

We are grateful for the financial support from the Vascular Training (VAST) Platform (TDR), the Canadian Institutes of Health Research (CIHR) (#PJT169688) and the Canada Research Chairs (CRC) program (JJC).

ABSTRACT

One of the most promising interventional targets for brain health is cerebral perfusion, but its link to white matter (WM) aging remains unclear. Motivated by existing literature demonstrating links between declining cortical perfusion and the development of WM hyperintensities, we posit that regional WM hypoperfusion precedes deteriorating WM integrity. Using the Human Connectome Project Aging (HCP-A) data set, we examine tract-wise associations between WM microstructural integrity (i.e. fractional anisotropy, mean diffusivity, axial diffusivity, and radial diffusivity) and perfusion (i.e. cerebral blood flow and arterial transit time) in ten major bilateral WM tracts. Results show that tracts displaying the largest CBF decline in aging do not necessarily display the largest ATT decline, and vice versa. Moreover, significant WM perfusion-microstructure canonical correlations were found in all tracts, but the drivers of these correlations vary by both tract and sex, with female subjects demonstrating more tracts with large microstructural variations contributing to the correlations. Additionally, arterial transit time appears to be the earliest indicator of WM declines, preceding age-related microstructural differences and CBF in several tracts. This study contributes compelling evidence to the vascular hypothesis of WM degeneration, and highlights the utility of blood-flow timing as an early marker of aging.

Keywords: White Matter, Aging, Diffusion, Perfusion, Microstructure, Tractography

1 INTRODUCTION

Increasing appreciation for the importance of cerebrovascular health in maintaining tissue integrity has led to the examination of tissue structure-perfusion associations in brain aging. The existing literature has focused largely on gray matter (GM) perfusion (Zhang et al., 2017) and its associations with cortical and subcortical atrophy (Baker et al., 2014; Chen et al., 2011, 2013; C.-M. Kim et al., 2020; Mayer et al., 2021). In the white matter (WM), microstructural declines in aging are reported in a robust body of literature, demonstrating regional differences in age-related microstructural declines along both broad regional and tract-specific segmentations (Baker et al., 2014; Bender et al., 2016; de Groot et al., 2015, 2016; Sala et al., 2012; Slater et al., 2019). Furthermore, recent investigation of tract-wise differences in patterns of microstructural and morphometric decline (Schilling et al., 2022), as well as in relationships between WM integrity and tract morphometry (Robinson et al., 2024), suggest that microstructural variations in different tracts are differentially associated with morphometric declines with age. However, the basis of this heterogeneity between tracts remains unclear. These findings cumulatively suggest that a more complete understanding of the interrelations between perfusion and integrity in the WM on a tract-specific basis is necessary to clarify patterns of decline across the brain.

A well-established relationship between cortical perfusion and the development of WM hyperintensities in associated subcortical regions illustrates the importance of CBF to maintaining the integrity of WM fibers (Bernbaum et al., 2015; O'Sullivan et al., 2002). Cortical perfusion was further related to subcortical WM integrity in normal aging (Chen et al., 2013). Relationships have been demonstrated between cortical perfusion and cognitive performance (D. Kim et al., 2021), and decreased cortical perfusion may predict heightened vulnerability to pathological declines (Chen et al., 2013; Mayer et al., 2021; O'Sullivan et al., 2002). However, regional variation in age-related cortical atrophy does not appear to match regional reductions in cerebral blood flow (CBF) (Chen et al., 2011; Tosun et al., 2010), suggesting a potential temporal asynchrony in perfusion and structural effects of age. Such an asynchrony, with perfusion decline preceding structural decline, would be consistent with the vascular hypothesis of aging and dementia (de la Torre, 2018), but has yet to be confirmed despite promising evidence that CBF

changes precede structural degeneration changes in the GM (Lee, 2022; Wierenga et al., 2014; Zlokovic, 2011). Moreover, investigations of this nature are much scarcer in the WM, despite the latter manifesting age effects earlier than GM (Giorgio et al., 2010). Existing research has demonstrated that trends of WM perfusion variations with age may differ significantly from those found in the GM, to the extent that the direction of perfusion change in aging is debated (Alisch et al., 2021; Damestani et al., 2024). Clarifying these regional patterns by tract will be necessary to understanding perfusion as a potential precursor to microstructural declines.

If it can be established that WM perfusion changes similarly lead microstructural degeneration, then regional perfusion in the WM itself can be a strong candidate as an early imaging marker of age-related declines in WM microstructure should, but the structural-perfusion relationship in the aging WM has not been examined. This paucity of work on WM perfusion is largely due to challenges in WM perfusion quantification (Bernbaum et al., 2015; Chen et al., 2013), the low vascularization and long arterial transit delays (ATT) in the WM as well as the presence of partial-volume effects with the GM. Recently, multi-delay pseudo-continuous ASL, which is better suited for WM perfusion mapping than conventional techniques, was used to demonstrate tract-specific declines in CBF and elongation in ATT (Damestani et al., 2024). Building on this development and incorporating regional perfusion measures into our ongoing model of WM microstructural and morphometric declines with age (Robinson et al., 2024), we aim to gain a more comprehensive understanding of how WM microstructural variations across age are related to perfusion parameters. To some extent, patterns of WM decline and resilience appear to broadly follow developmental trajectories, though support for ordered models is mixed (Hoagey et al., 2019; Slater et al., 2019; Stricker et al., 2009), prompting a tract-wise approach. Given the previously limited ability to measure regional differences in WM perfusion (Bernbaum et al., 2015; Chen et al., 2013) and the sparsity of studies addressing WM vascular-microstructural declines on a tractwise basis (Mayer et al., 2021; Smirnov et al., 2021), this study aims to fill both of these knowledge gaps, with the understanding that WM tracts represent the meaningful structural units for segmentation of the WM (Baker et al., 2014; Sala et al., 2012; Yeatman et al., 2014) in aging, as well as reflecting functional

connections between terminal cortical regions (Nozais et al., 2021). As variability in tractwise perfusion remains underexplored in healthy adults, it represents a natural extension to the existing literature and a valuable missing component in modeling regional WM declines with age and may represent an underlying source of differences in order and rate of tractwise declines. Using the Human Connectome Project Aging (HCP-A) data set (Bookheimer et al., 2019), this study sought to map tractwise age-related variations in WM perfusion, as well as the relationships between tractwise WM perfusion and microstructure. We hypothesized that (1) tract perfusion and microstructure will not decline at the same rate at aging, and that (2) tractwise perfusion changes will be detectable at younger ages than microstructural declines.

2 METHODS

This study includes five hundred and thirty-five healthy adult subjects (300 female, aged 36-100) from the Human Connectome Project in Aging (HCP-A) dataset (OMB Control# 0925-0667 (Bookheimer et al., 2019; Harms et al., 2018). All subjects were in generally good health and without pathological cognitive impairment (i.e. stroke, clinical dementia). Following manual quality control, thirty-two subjects were excluded from this sample due to MRI artifacts that produced notable errors when generating WM masks. Three additional subjects were excluded as age outliers due to being the only subjects of 100 years of age. Thus, the final sample size was 500 subjects (294 female, aged 36-89, aprox. 59% postmenopausal (Gold, 2011)). Hypertension status was determined based on mean arterial pressure (Kandil et al., 2023).

Table 1: Sample Demographics
Demographic statistics for all subjects, female subjects, and male subjects. All subjects were in good health and without pathological cognitive impairment (i.e. stroke, clinical dementia).

	Count	Mean Age (years)	Median Age (Years)	Age Range (Years)	Age Stdev (Years)	Hypertension Count (<60 y/o)	Hypertension Count (≥60 y/o)	Education (years)
All	**500**	**57.88**	**56**	**36-89**	**14.3**	**75**	**59**	**17.41**

Female	294	57.27	54	36-89	14.4	37	26	17.29
Male	206	58.76	58	36-89	14.2	38	33	17.58

The study accessed whole-brain T1-weighted structural MRI, diffusion-weighted MRI (dMRI) with a $(1.5mm)^3$ voxel resolution, MB=4, with 93 directions at $b=1500s/mm^2$, and multi-delay multi-band echo planar imaging (MB-EPI) pseudo-continuous arterial spin labeling (pCASL) with a $(2.5mm)^3$ voxel resolution, MB=6, with TIs = 0.7, 1.2, 1.7, 2.2, and 2.7, collected using four matched Siemens Prisma 3T MRI scanners. Further imaging parameters for structural, diffusion, and perfusion imaging can be found in (Harms et al., 2018).

2.1 Image analysis

dMRI data were corrected for eddy-current and susceptibility-related distortions via EDDY prior to use in tractography analysis. Eighteen major WM tracts were reconstructed from the dMRI data using the Tracts Constrained by Underlying Anatomy (TRACULA) tool in Freesurfer version 7.2.0 (Maffei et al., 2021; Yendiki et al., 2011). Tracts reconstructed by TRACULA's trac-all command represent pathways in which each adjacent voxel has a 99% probability of containing the next step in the fibre pathway of interest, ensuring the highest level of anatomical feasibility while excluding potential WM hyperintensities. Prior to extracting diffusion values, all values below 20% of the maximum posterior probability distribution were thresholded (Maffei et al., 2023). The TRACULA pipeline also incorporates

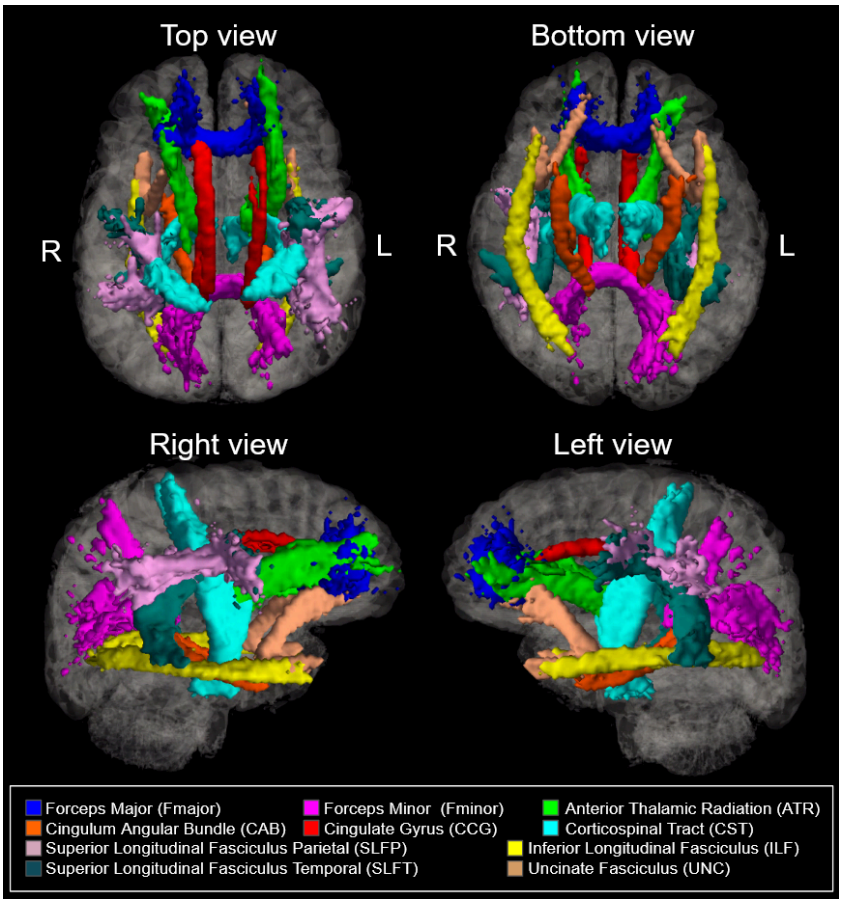

***Figure 1**: Ten bilateral tracts of interest reconstructed Freesurfer's TRACULA package. Note that there is limited overlap between tracts.*

correction for eddy current distortion, brain extraction, tensor calculation, and affine registration. Per-subject DTI and Perfusion images were registered in local space using Freesurfer's TKRegister function. FSL's fslmaths function was then used to produce per-subject masks of each WM tract in local space from the full TRACULA tract volumes. The eighteen reconstructed tracts were combined bilaterally to produce ten tracts of interest for analysis: The major forceps (Fmajor), minor forceps (Fminor), anterior thalamic radiation (ATR), cingulum angular bundle (CAB), cingulate gyrus (CCG), corticospinal tract (CST), inferior longitudinal fasciculus (ILF), superior longitudinal fasciculus parietal (SLFP), superior longitudinal fasciculus temporal (SLFT), and the uncinate fasciculus (UNC) (**Figure 1**). Rosner's tests were performed to identify and exclude volume outliers per tract in single tract analyses. The resulting subject counts for these analyses were: Fmajor (N=493), Fminor (N=493), ATR (N=497), CAB (N=490), CCG (N=495), CST (N=491), ILF (N=497), SLFP (N=497), SLFT (N=495), and UNC (N=495).

2.1.1 Microstructure

WM microstructural integrity was quantified using fractional anisotropy (FA), mean diffusivity (MD), axial diffusivity (AD), and radial diffusivity (RD). FA, MD, AD, and RD maps were derived via

Dipy's DKI script to achieve kurtosis-corrected DTI metric fitting, due to the high b-value used in the HCP-A acquisitions. TRACULA generated tract masks were applied to local dMRI images in flsmaths to generate tract means for FA, MD, AD, and RD. For each metric, we defined the "baseline" as being measured from the youngest 10% of the group, and computed baseline normalized (percent of baseline) values ("FA_{perc}", "MD_{perc}", "AD_{perc}", "RD_{perc}"). These were defined as individual raw tract values divided by the mean raw tract value of these youngest subjects to assess percent differences from the youngest baseline, with separate baseline calculations performed for female and and male subsets of the sample (**Figure 2a**).

2.1.2 Perfusion

Perfusion metrics of interest to this study included cerebral blood flow (CBF) and arterial transit time (ATT). A separate calibration scan was used to measure M0, which was used in CBF quantification. The pCASL label elevated the WM SNR relative to conventional pulsed ASL methods. Multi-TI data were fit to the general kinetic model (implemented through FSL's oxford_ASL command) to produce local CBF and ATT maps (Wang et al., 2013). Partial volume correction was applied to the local maps. Specifically, the T1-weighted structural image for each subject was segmented, from which GM and WM partial volume estimates were extracted and transformed into the same space as the ASL images. GM and WM masks were generated using empirically chosen thresholds of 0.75 and 0.9, respectively, and applied to the estimated CBF images within which the mean estimated CBF and its standard deviation estimate were calculated. Separate gray and white matter T1s are used in the kinetic model inversion. Multi-tissue T1 values were adopted from the literature to account for partial-volume effects. Thus, the use of multi-TI pCASL with partial-volume correction addresses the challenges of long ATT, low SNR and partial-voluming in WM perfusion mapping.

As with microstructure, TRACULA-generated tract masks were applied to the local maps in fslmaths to produce tract means for both perfusion metrics. Baseline normalized perfusion values ("CBF_{perc}", "ATT_{perc}") were again calculated as individual raw tract values divided by the mean raw tract

value of the youngest 10% of subjects (i.e. the baseline group) using the same female and male subsets as previous baseline.

2.2 Statistical analysis

2.2.1 Age and sex effects

Between-subjects ANOVA was used to determine the presence of sex differences in tract specific FA_{perc}, MD_{perc}, CBF_{perc}, and ATT_{perc}. Subsequent assessment of sex differences in microstructure and perfusion were conducted for each tract via sequential multivariate regressions of sex on to mean FA_{perc}, MD_{perc}, CBF_{perc}, and ATT_{perc} using age as a covariate of no interest. Whole-WM age-related microstructure and perfusion differences were assessed via multivariate quadratic regression by first regressing age onto mean FA_{perc}, MD_{perc},CBF_{perc}, and ATT_{perc} values derived from voxel-count weighted tract averages using sex as a covariate of no interest. This process was repeated for each tract separately in tract-wise analyses. FDR adjustment was again applied to the resulting p-values. Sex differences in age effects on tractwise FA_{perc}, MD_{perc},CBF_{perc}, and ATT_{perc} were assessed using multivariate regression of sex, age and the age-sex interaction.

2.2.2 Microstructure vs Perfusion

Two multivariate regression models were constructed to assess relationships between microstructure, perfusion, age, and sex in our sample. Both models were applied first to whole-WM MD_{perc} and FA_{perc} values, then to each tract:

- *Model 1. microstructure vs. perfusion across ages:* assesses the degree to which perfusion metrics account for the age-related variability in mean normalized tract MD and FA, with subject sex as a covariate of no interest. That is,
    - $\{FA_{perc}, MD_{perc}\} = f(CBF_{perc}+Sex)$
    - $\{FA_{perc}, MD_{perc}\} = f(ATT_{perc}+Sex)$

- *Model 2. microstructure vs. perfusion between sexes:* assess the degree to which perfusion metrics account for sex-related differences in normalized tract MD and FA, with subject age as a covariate of no interest. That is,
    - $\{FA_{perc}, MD_{perc}\} = f(CBF_{perc}+Age)$
    - $\{FA_{perc}, MD_{perc}\} = f(ATT_{perc}+Age)$
    - One set of models is produced for each sex.

The above analyses were conducted in R (version 4.1.1). False Detection Rate (FDR) multiple comparison corrections were conducted on a per-model basis for all regressions.

2.2.3 Multimodal associations: Canonical correlation analysis (CCA)

Canonical correlation analysis (CCA) was conducted to examine the degree to which each of our variables of interest contributed to associations between microstructure and perfusion, respectively. CCA allows the creation of linear combination vectors of multiple related measures to examine the degree of contribution (or loading) of each constituent variable to the relationship between the tested vectors. Two column vectors were computed using our perfusion (V_1) variables (CBF_{perc}, ATT_{perc}) and microstructural (U_1) variables (AD_{perc}, RD_{perc}, FA_{perc}) in Matlab. The linear combinations of V and U vectors which produced the highest correlation were then calculated to determine on a tractwise basis which variables loaded most strongly to correlated (between perfusion and microstructure) age differences by tract. Values more than three scaled median absolute deviations (*Difference of Median*, n.d.) from the median were excluded for each measure prior to CCA analysis. Split-half cross-validation was conducted through 10,000 permutations of random sampling of the male and female data sets. CCA was performed on each of the 10,000 randomly split samples, and mean and standard error of loadings associated with only statistically significant canonical correlations are plotted to confirm consistency of the CCA findings.

2.2.4 Age-displaced analysis: cross-correlation function (CCF)

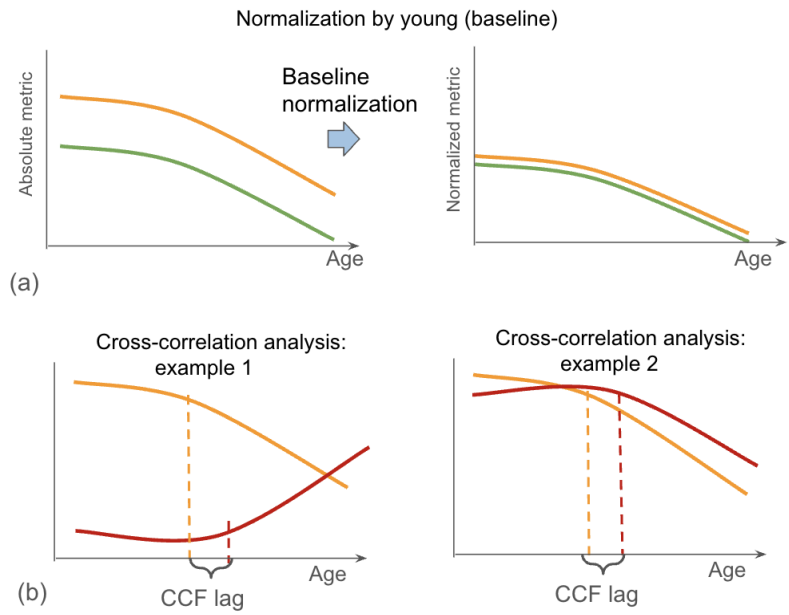

***Figure 2**: Illustration of a) relative effects of baseline normalization on study metrics to produce FA_{perc}, MD_{perc}, AD_{perc}, RD_{perc}, CBF_{perc}, and ATT_{perc} values, as well as b) interpretation of peak offset in cross correlation analysis.*

Cross-correlations functions (CCF) were calculated in Matlab (Mathworks, Natick, USA) to determine the presence of shifted correlations across measures for perfusion and microstructure. In the absence of longitudinal data, cross-correlation allows the examination of associations between variables at different points along cross-subject age-related trajectories, and the generation of hypotheses that could be tested longitudinally. In this work, a positive peak-correlation shift in variables A relative to variable B, indicates that variations in B are observable before they are observable in variable A (**Figure 2b**). Only variables demonstrating significant non-linear age effects on a tractwise basis were examined in this analysis to reduce ambiguity in CCF interpretation. A curvature threshold for age effects of 0.0005 was implemented, where curvature was computed using Matlab's *curvature* function. CCFs were calculated based on the models of age effects for six paired tractwise microstructure/morphometry measures, along with cross-comparisons for AD_{perc}/RD_{perc} vs FA_{perc} and CBF_{perc} vs ATT_{perc}:

- CBF vs. Microstructure: CBF_{perc} vs AD_{perc}, CBF_{perc} vs RD_{perc}, CBF_{perc} vs FA_{perc}
- ATT vs. Microstructure: ATT_{perc} vs AD_{perc}, ATT_{perc} vs RD_{perc}, ATT_{perc} vs FA_{perc}
- AD_{perc} vs FA_{perc}
- RD_{perc} vs FA_{perc}
- CBF_{perc} vs ATT_{perc}

3 RESULTS

3.1 Age differences

Significant linear and quadratic relationships between age and CBF_{perc} were identified in all tracts but UNC, with quadratic regressions providing a better fit as indicated by higher $R^2_{adjusted}$ in all tracts with the exception of Fminor and CCG. Significant associations were also identified between age and ATT_{perc} in Fmajor, ILF, and UNC, along with significant linear effects in Fminor, ATR, CCG, CST, SLFP, SLFT, and UNC, with quadratic regression providing a better fit in UNC. Significant linear and quadratic relationships between age and MD_{perc} were identified in all tracts of interest, with quadratic regressions providing a better fit in all tracts. Lastly, significant quadratic associations between age and FA_{perc} were found in Fminor, CCG, and ILF, with significant linear associations in Fmajor, Fminor, ATR, CAB, CCG, ILF, SLFP. Quadratic regression provided a better fit for the effects of age on FA in Fminor and CCG (**Figure 3**).

To further verify the viability of ATT estimation in the WM, we found that across subjects, both CBF and ATT values in the whole WM were linearly associated with those across the whole GM (**Supplementary Figure 1**). Linear regression of GM CBF/ATT as a function of WM CBF/ATT returned a strong association between tissue types: slope = 0.13 (WM CBF vs. GM CBF), intercept = 2.4, $F(1, 498) = 633.4$, $p < .001$, $R^2_{Adjusted} = .56$; slope = 0.26 (WM ATT vs. GM ATT), intercept = 1.3, $F(1, 498) = 256.5$, $p < .001$, $R^2_{Adjusted} = .34$. Notably, WM ATT was on average 1.3 s longer than GM ATT, which is consistent with the range published in the literature (Juttukonda et al., 2021; van Osch et al., 2009).

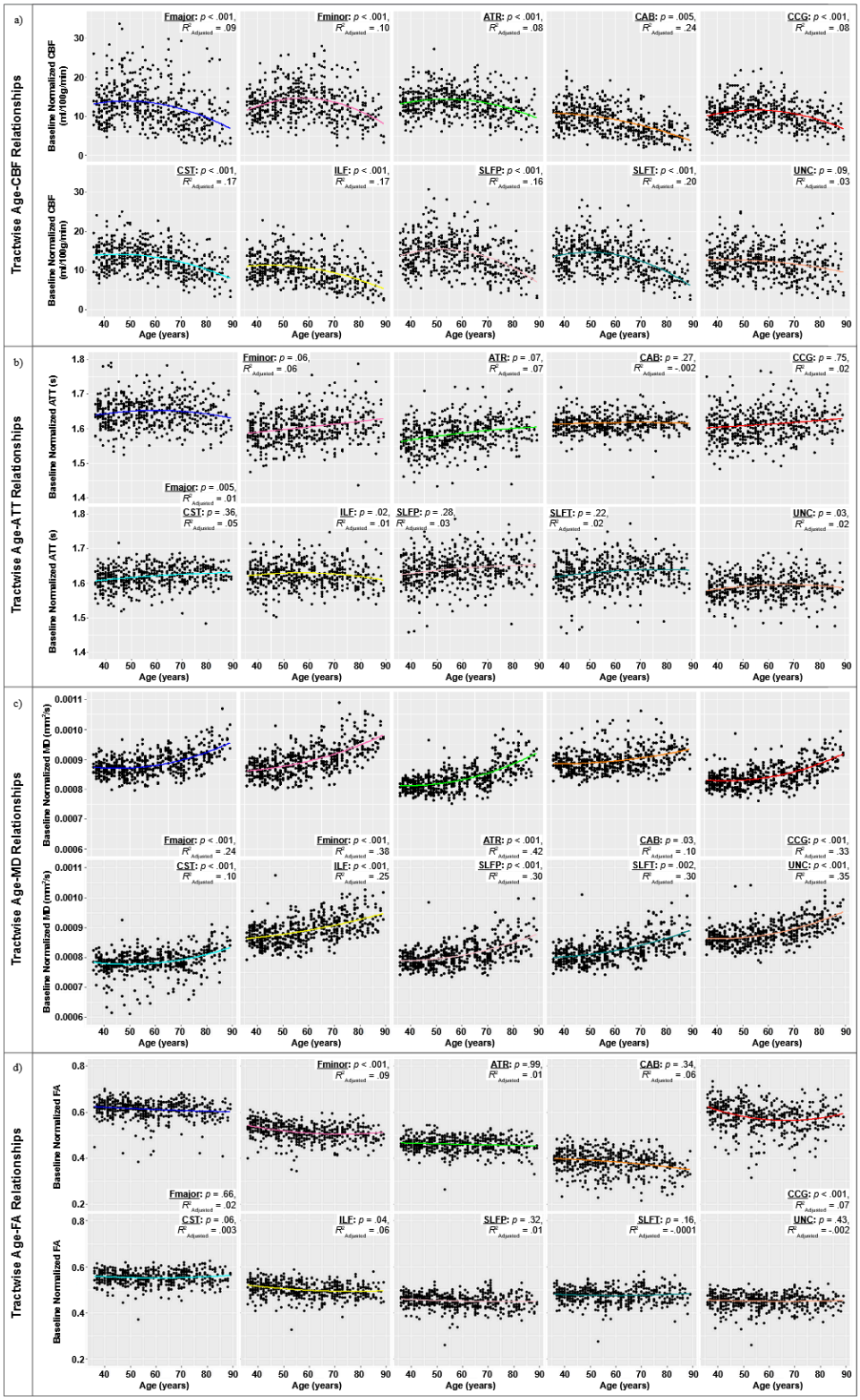

Figure 3: *Tractwise quadratic regression of age effects on baseline normalized CBF, ATT, MD, and FA, with each dot representing one subject. The p-values and effect sizes (R2adjusted) from the quadratic fit are noted for each tract.*

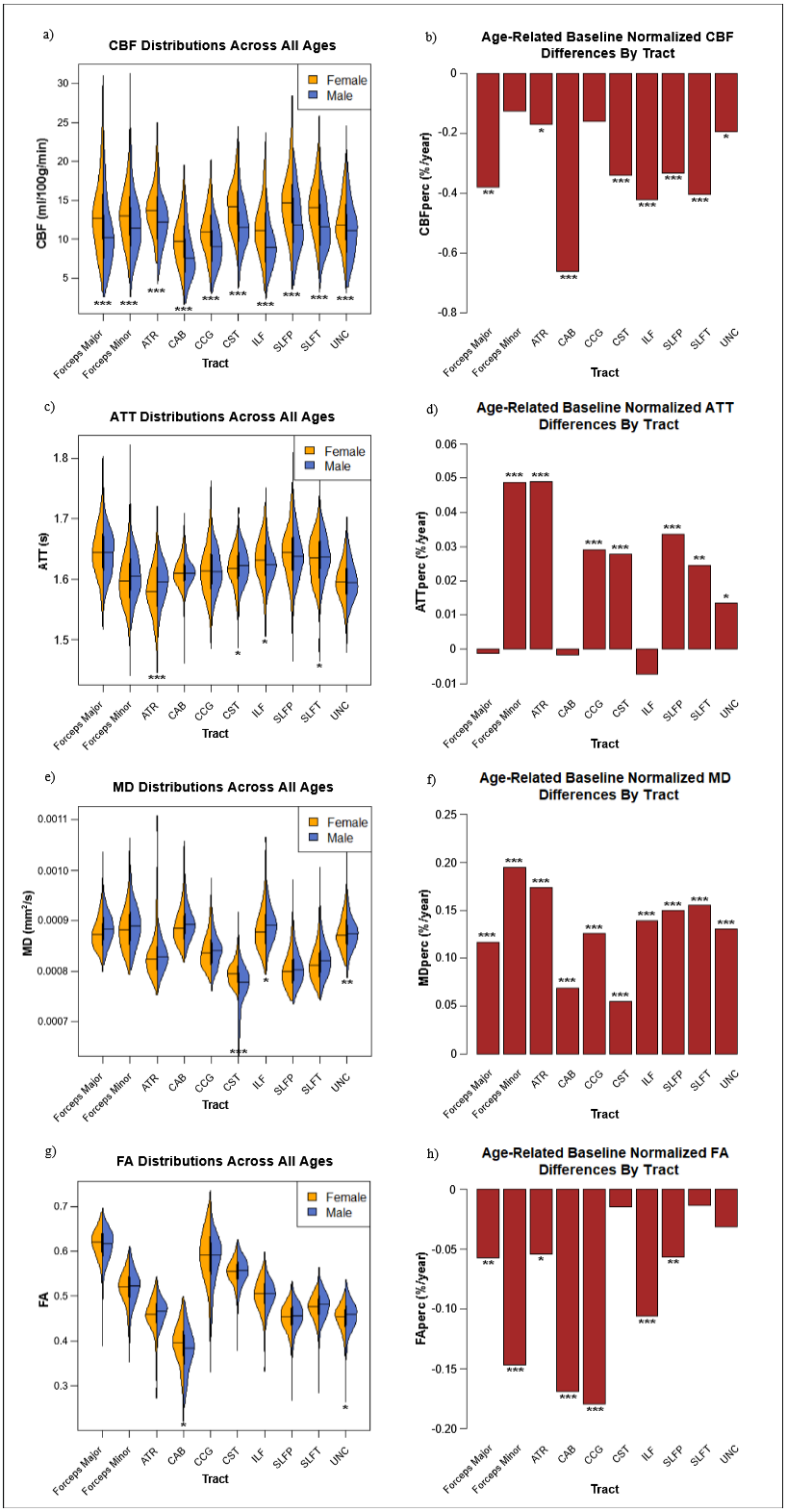

Figure 4: *Raw distributions separated by sex (a,c,e,g) and tractwise age effects (b,d,f,h) for CBFperc, ATTperc, MDperc, and FAperc respectively. Significant effects by sex and age are denoted with asterisks (*:p<.05, **:p<.01, ***:p<.001)*

3.2 Sex differences

Prior to baseline normalization, higher raw MD was found in female subjects in the CST, and in male subjects in the ILF and UNC. FA differences were similarly mixed where significant, with female subjects showing higher FA in the CAB, and male subjects showing higher raw FA in the UNC. More consistent sex differences were found in CBF, with female subjects showing higher raw CBF in all tested tracts, corroborating previous research on sex differences in cortical perfusion (Y. Liu et al., 2012; Tosun et al., 2010). However, raw ATT values again demonstrated tract dependence in sex differences, with longer raw ATT in female subjects in the ILF, and longer raw ATT in male subjects in the ATR, CST, and SLFT (**Figure 4**).

Following baseline normalization, female subjects showed significantly higher MD_{perc} in the Fmajor, ATR, CST, ILF, SLFP, and SLFT in regression analysis. That is, these tracts may demonstrate more microstructural decline with advancing age than the others. While female subjects also demonstrated higher FA_{perc} in the Fmajor, male subjects showed higher FA_{perc} in the Fminor, CCG, SLFP, and SLFT. Female subjects demonstrated higher CBF_{perc} in the CAB, while male subjects showed higher CBF_{perc} in the ATR. Female subjects showed higher ATT_{perc} in the SLFP and SLFT, while male subjects showed higher ATT_{perc} in the ILF.

Significant age-sex interactions were identified for MD_{perc} in the Fminor ($F(2, 489) = 70.8$, $p = .007$, $R^2_{Adjusted} = .30$), ATR ($F(2, 493) = 76.9$, $p = .009$, $R^2_{Adjusted} = .29$), CAB ($F(2, 486) = 11.5$, $p = .046$, $R^2_{Adjusted} = .06$), and UNC ($F(2, 491) = 47.3$, $p = .015$, $R^2_{Adjusted} = .22$), such that in all instances, female subjects exhibited greater MD increases in aging. Interactions of age effects by sex were also found in FA_{perc} in the ATR ($F(2, 493) = 4.37$, $p = .013$, $R^2_{Adjusted} = .02$), SLFP ($F(2, 493) = 6.03$, $p = .009$, $R^2_{Adjusted} = .03$), and SLFT ($F(2, 491) = 5.60$, $p = .001$, $R^2_{Adjusted} = .03$), with greater FA_{perc} decreases in aging for female subjects. Interactions of age by sex for CBF differences were only identified in the CCG ($F(2, 491) = 2.49$, $p = .042$, $R^2_{Adjusted} = .009$), such that CBF_{perc} declines were greater in female subjects. No interactions by subject sex were found in age-related ATT_{perc} differences.

3.3 Microstructure-perfusion relationships

3.3.1 Regression analyses

Model 1 (perfusion vs microstructure): Significant relationships were identified between CBF_{perc} and MD_{perc} ($F(2, 497) = 5.36$, $p = .005$, $R^2_{Adjusted} = .02$, slope = -0.02), as well as between ATT_{perc} and MD_{perc} ($F(2, 497) = 4.07$, $p = .02$, $R^2_{Adjusted} = .01$, slope = 0.23). No significant whole-WM relationships were found between FA_{perc} and WM perfusion (**Supplementary Table 1a**).

Significant negative relationships were found between tractwise CBF_{perc} and MD_{perc} in the ILF and SLFT. Significant positive relationships between ATT_{perc} and MD_{perc} were identified in the Fminor, ATR, SLFP, and SLFT. A single significant positive association was found between CBF_{perc} and FA_{perc} in the CCG. A significant negative relationship between ATT_{perc} and FA_{perc} was identified in the ATR, along with a positive relationship in the CAB Tract-wise results are summarized in **Supplementary Table 1b**.

Model 2 (sex differences in perfusion-microstructure relationships): No significant relationships were identified between whole-WM microstructure and perfusion in Model 2 (**Supplementary Table 2a**). After dividing the sample by sex, significant positive associations were found between CBF_{perc} and FA_{perc} in the CCG in both female and male subjects, as well as in the ATR in female subjects alone. A single negative association between CBF_{perc} and FA_{perc} was found in the CST in male subjects. Female subjects also demonstrated both a negative association between ATT_{perc} and FA_{perc} in the ATR, and a positive association between ATT_{perc} and FA_{perc} in the CAB. No associations were identified between perfusion and MD after dividing the sample by sex. Tract-wise results are summarized in **Supplementary Table 2b.**

3.3.2 Multimodal associations based on CCA

The CCA identified a common pattern of association between microstructure and perfusion loadings in male and female subjects in several tracts (**Figure 5**). Loadings are listed for significant canonical correlations ($p < 0.05$) using a loading threshold of 0.3. In female subjects, CBF_{perc} contributed significantly in six tracts (ATR, CCG, CST, ILF, SLFP and UNC), while ATT_{perc} did not contribute significantly to perfusion-microstructure associations in any tract. Across tracts, AD_{perc} and RD_{perc} were

not found to load significantly, while FA_{perc} loaded significantly in four tracts (Fminor, ATR, CCG and UNC). Three tracts demonstrated significant loading by both CBF_{perc} and FA_{perc} (ATR, CCG, UNC) in females.

In male subjects, CBF_{perc} also contributed significantly to the perfusion-microstructure relationship in six tracts (ATR, CCG, CST, ILF, SLFP, SLFT), while FA_{perc} co-contributed significantly in only one tract (CCG). The CCG was also the only tract displaying significant loading by both CBF_{perc} and FA_{perc} for males. No other measures demonstrated significant loading in male subjects. In both sexes, FA_{perc} was the only microstructural parameter to contribute to these relationships, while CBF_{perc} showed the only significant perfusion loading.

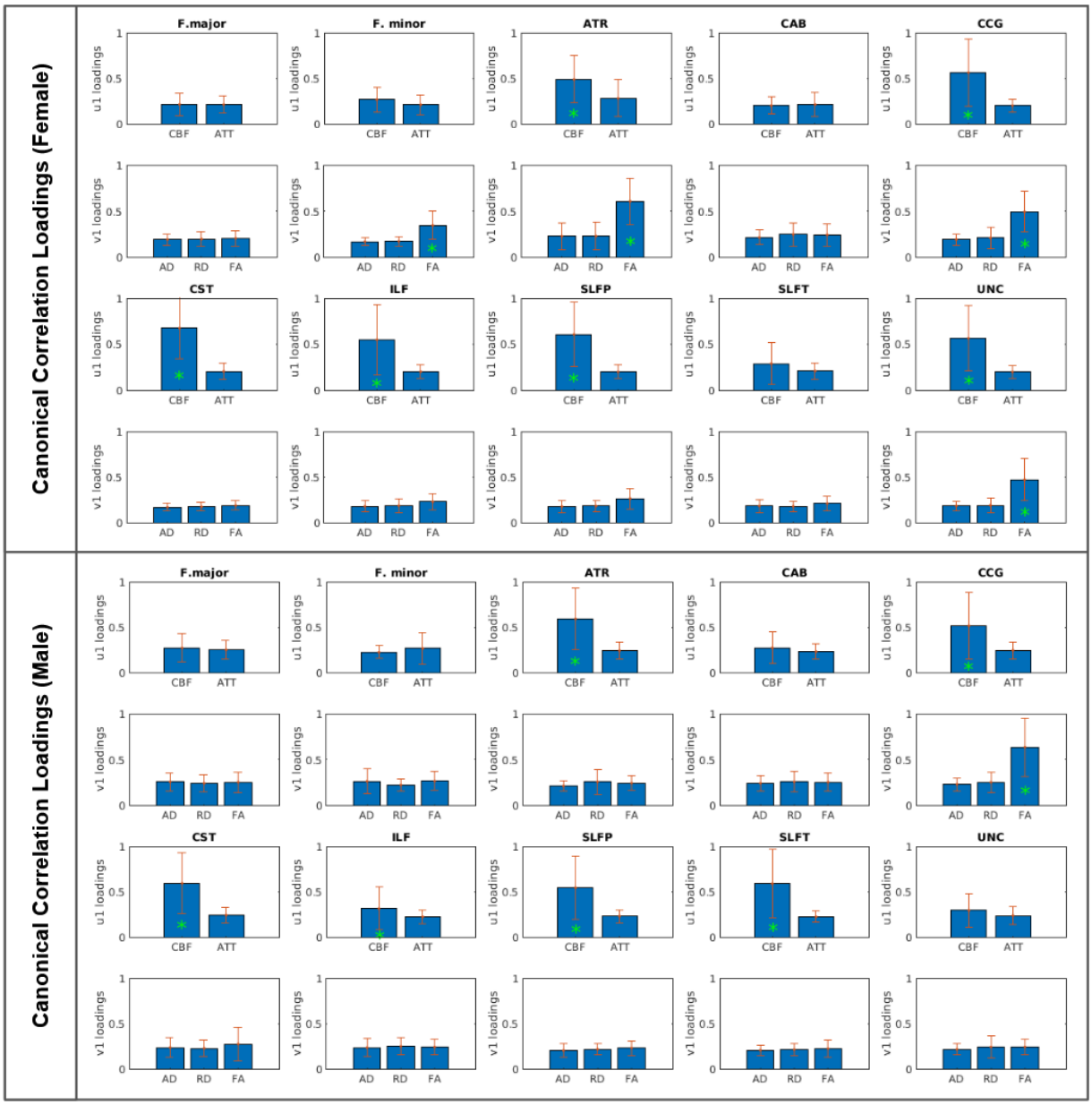

***Figure 5**: Tract-wise contributions by all perfusion (CBF_{pere}, ATT_{pere}) and microstructural (AD_{pere}, RD_{pere}, FA_{pere}) measures to categorical perfusion-microstructural relationships in aging. U1 and V1 refer to latent variables related to perfusion and microstructure, respectively. Green asterisks denote the loading threshold of 0.3.*

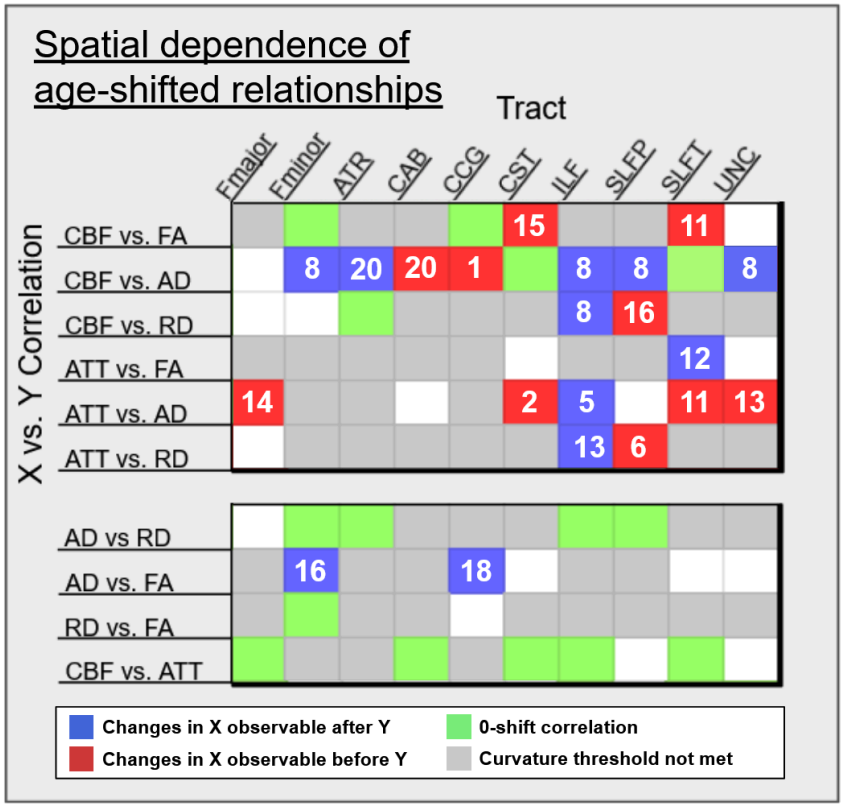

***Figure 6**: Tractwise cross-correlation results demonstrating significant peak correlations ($p < .05$) for pairs of perfusion and microstructural variables at positive, negative and zero correlational shift. While cells indicate no significant association between measures. Length of peak-offset in years (approx.) is included in relevant cells.*

3.3.3 CCF results of age-displacement analysis

Correlating perfusion and microstructure measures across age shifted timeseries identified a broad ordered trend in earliest detectable ages of change of ATT_{perc}, followed by AD_{perc}, then CBF_{perc} and the remaining microstructural measures, in addition to considerable tractwise differences. Significant correlations at zero peak-correlational shift were observed between CBF_{perc} and FA_{perc} in Fminor and CCG, between CBF_{perc} and AD_{perc} in CST and SLFT, and between CBF_{perc} and RD_{perc} in the CAB. Significant associations at a positive peak-correlation shift were found in CBF_{perc} relative to FA_{perc} in CST and SLFT; between CBF_{perc} and AD_{perc} in CAB, and CCG; and between CBF_{perc} and RD_{perc} in the SLFP, such that CBF_{perc} changes were observable at earlier ages than FA_{perc}. In other words, in these tracts, variations in CBF_{perc} were observable before those in FA_{perc} and AD_{perc}. Similarly, significant correlations at positive shift between ATT_{perc} and AD_{perc} were found in Fmajor, CST, SLFT, and UNC; and between ATT_{perc} and RD_{perc} in the SLFP, such that variations in ATT_{perc} were observable before those in AD_{perc} or RD_{perc}. Significant correlations at negative shift were found between CBF_{perc} and AD_{perc} in Fminor, ATR, ILF, SLFP, and UNC, as well as between CBF_{perc} and RD_{perc} in the ILF alone, such that variations in CBF_{perc} were observable after those in AD_{perc} or RD_{perc}. Significant correlations at negative shift were also found between ATT_{perc} and FA_{perc} in the SLFT; between ATT_{perc} and AD_{perc} in Fmajor, CST,

SLFT, and UNC; and between ATT_{perc} and RD_{perc} in the ILF_{perc} alone such that changes in ATT_{perc} were observable at later ages than changes in FA_{perc}, AD_{perc}, or RD_{perc} respectively (**Figure 6**).

Comparisons within perfusion and microstructure measures respectively found significant correlations at zero shift between AD_{perc} and RD_{perc} in Fminor, ATR, ILF, and SLFP; as well as between RD_{perc} and FA_{perc} in the Fminor. In perfusion measures, significant zero-shift correlations were found between CBF_{perc} and ATT_{perc} in Fmajor, CAB, CST ILF, and SLFT. Additionally, two significant correlations at negative peak shift were identified between AD_{perc} and FA_{perc} in Fminor and CCG, such that changes in AD_{perc} were observable at earlier ages than changes in FA_{perc}.

4 DISCUSSION

We initially hypothesized that (1) tractwise microstructural and perfusion declines would not progress at the same rate in aging due to (2) earlier detectable declines in WM perfusion than microstructural integrity. Our findings support Hypothesis 1 and in part Hypothesis 2, but also highlight the fact that the patterns of decline were much more varied by tract, sex and by measure than initially stated in Hypothesis 2.

MD was largely found to increase quadratically with age, while FA declined linearly in the majority of tracts. While this finding is in broad agreement with the aging literature (de Groot et al., 2016; Giorgio et al., 2010; Slater et al., 2019), FA was not uniformly associated with age across tracts, indicating variability in patterns or rates of WM decline. Across sexes, our microstructural results provide partial support for fronto-temporal tracts declining at a higher rate than those in the posterior WM (**Figure 4**). We also found significant and consistent CBF and ATT associations with age. Specifically, CBF declines quadratically with advancing age in the vast majority of WM tracts, somewhat mirroring the age-associated increases in tractwise MD (**Figure 3**), with the quadratic behaviour consistent with previous findings by Juttukonda et al. in the same cohort (Juttukonda et al., 2021). CBF appears to demonstrate a peak in middle-age, with the peak location varying by tract. Moreover, ATT demonstrates a robust linear increase with advancing age, consistent with previous reports (Mutsaerts et al., 2015).

Importantly, we found a tendency for ATT to lead microstructural metrics in age-related variations. Nonetheless, this effect is tract-dependent, which may be explained by the tract-dependent cellular and vascular developmental processes.

4.1.1 Tract-based approach

With regards to vascular development, vessels in frontal and cerebrospinal tracts develop in the embryo prior to those in the parietal and posterior brain, supporting the development of their respective WM regions (Smirnov et al., 2021). This raises vascularization differences as a potential source of differences in rates and patterns of WM declines. These lines of evidence encourage a tract-wise determination of perfusion-microstructural associations, whereby those tracts or regions that demonstrate greater robustness to age-related microstructural declines may be distinguished by vascular factors that are potentially related to the manner in which blood vessels developed. Unlike the cortical surface, which is fed by larger penetrating vessels, blood supply to the WM is fed primarily by smaller vessels entering from either the cortical surface or the midbrain (Nonaka et al., 2003; Smirnov et al., 2021). This results in both (1) considerable variation in proximity to major vessels and number of blood flow sources and (2) the likelihood that vascular disease and age-related deterioration that differentially affects small vessels has an earlier impact on the WM than on the cortical surface (Akashi et al., 2017; Hase et al., 2018). Tractwise heterogeneity in blood vessel development may then underlie susceptibility to age-related changes in perfusion and regional ability to support microstructural integrity in adulthood.

Thus, we took a tract-wise approach that complements recent work based on a voxel-wise approach (Damestani et al., 2024). While prior findings have indicated regional gains in WM CBF with aging (Alisch et al., 2021), we found significant trackwise CBF declines. The highest age effects on CBF appear to manifest in Fmajor, CAB, ILF and SLFT, suggesting higher rates of vascular decline in the temporo-posterior WM than more anterior-superior tracts such as the Fminor or CCG which demonstrate little to no CBF declines with age. Thus, vascular age effects do not appear to follow the current retrogenesis models that predict earlier or more rapid age declines in anterior regions (Brickman et al.,

2012; Slater et al., 2019; Vik et al., 2015). However, patterns of age-related ATT increases across our tracts do not follow this pattern. Despite showing some of the greatest CBF declines, Fmajor, CAB, and ILF tracts exhibited no significant ATT increases with age. This pattern is in line with the voxelwise findings by Damestani et al. (Damestani et al., 2024), and suggests that ATT and CBF cannot be considered interchangeable measures of microvascular decline, and instead reflect different signatures or stages of microvascular aging that will require targeted analysis to clarify.

4.1.2 Understanding different types of WM-perfusion associations through multimodal integration

As revealed by the CCA, the interrelation between perfusion and microstructural integrity varied by tract. This highlights the importance of investigating the regional heterogeneity in the interplay between vascular and structural declines. Moreover, rather than a smooth shared trajectory of decline, our evidence indicates the presence of different combinations of age effects: (i) significant loadings by CBF_{perc} alone; (ii) significant loading by FA_{perc} alone; (iii) significant loadings by CBF_{perc} and FA_{perc} **(Figure 5**). In most cases, CBF_{perc} and FA_{perc} loaded in the same direction, consistent with the global relationship shown by Damestani et al. (Damestani et al., 2024). However, several tracts (Fmajor, CAB and SLFT in females, Fmajor, Fminor, CAB and UNC in males) did not show significant loading contributions by either microstructural or perfusion metrics. An interesting follow-up question is, given the obvious differences in variables such as perfusion and axonal diameter across these tracts, what mechanism(s) may be driving the heterogeneity in the perfusion-microstructural associations?

Notwithstanding, the understanding of the WM aging process appears to be generalizable across all WM. For example, using the CST as a point of reference for a tract presumed to survive relatively robustly into later age (Michielse et al., 2010), we see that the CST exhibits the lowest MD increases and no significant differences in FA with age, despite sizable CBF_{perc} and ATT_{perc} age effects. As axon diameter comparisons across the WM have observed relatively high mean diameter in CST fibers (Fan et al., 2020; Liewald et al., 2014), fiber diameter in healthy WM may be a predictor for resilience to perfusion declines. Additionally, tracts with different mean axon diameters (Fan et al., 2020; Gast et al.,

2023) are accompanied by differing metabolic demands (Harris & Attwell, 2012). One possibility for this is that the metabolic cost of maintaining myelin itself scales with fiber diameter, so thicker fibers, such as those of the CST may be less metabolically sensitive than those with thinner fibres, such as the UNC. Nonetheless, the driver of sex-related differences in these vascular-microstructural differences remain unclear.

4.1.3 Sex differences in perfusion-microstructural covariations

In addition to perfusion-microstructure associations differing by tract, they also varied considerably between sexes (**Figure 5**). First, female subjects have poorer WM integrity as a group, as shown by the higher group-averaged MD_{perc} and lower FA_{perc} values (**Figure 7**), and as shown previously (Inano et al., 2011; Intzandt et al., 2023; Lawrence et al., 2021). Females also tend to have higher CBF_{perc} (consistent with previous findings (Alisch et al., 2021)) and shorter ATT_{perc} (in anterior tracts) compared to males (**Figure 4**). Specific to multi-delay pCASL-based findings, these are similar to observations by Damestani et al. (Damestani et al., 2024; Juttukonda et al., 2021), although our values are normalized by the youngest group and separately for each sex, implying that in addition to sex differences in regional baseline (young) values, the regional age-related variations are also sex dependent. Moreover, female subjects demonstrated a greater number of tracts with significant relationships between WM microstructure and perfusion. This finding is consistent with previous reports of more rapid WM aging in females (Intzandt et al., 2023; Patel et al., 2023). We speculate that a likely cause of these differences in WM aging by sex are the effects of menopause on brain health more broadly. Menopause has previously been found to affect structural, connectivity, and metabolic measures in the brain (Mosconi et al., 2021).

Tractwise Sex Differences in Group-Mean Microstructural/Perfusion Measures (Covaried for Age)
Significant differences are colored. Red: Female>Male. Blue: Male>Female.

Tract	MD_{perc}	FA_{perc}	CBF_{perc}	ATT_{perc}
Fmajor				
Fminor				
ATR				
CAB				
CCG				
CST				
ILF				
SLFP				
SLFT				
UNC				

***Figure 7**: Tractwise sex differences in baseline normalized CBF, ATT, MD, and FA.*

Notably, cognitive impacts appear to stabilize post-menopause, though this is speculated to be the result of compensatory effects, rather than improvement in structural integrity. The sex differences with age observed in this study likely capture structural and microvascular impacts of peri- and postmenopause on the WM, though direct associations between these declines and cognitive performance will require additional investigation. Should microvascular declines be associated with cognitive performance similarly to the microstructural associations identified in this study, targeting vascular declines may benefit the study of interventions in the impacts of menopause on the brain in addition to the aging brain more generally. The degree to which hormone supplementation therapies may mitigate these effects, and indeed the mechanisms of estrogen's effects on WM health more generally, will require further investigation.

4.1.4 Temporal relationship in perfusion-microstructural variations in aging

Vascular declines with age have been consistently demonstrated in the WM as part of general systemic vascular decline (Kohn et al., 2015; Y. Li et al., 2018; Tomoto et al., 2023). Increasing arterial stiffness due to the progressive decay of elastin in normal aging results in more fragile blood vessels (Kohn et al., 2015; Tomoto et al., 2023). Even in intact arterial pathways, changes in vessel morphometry result in more tortuous micro- and mesovasculature with reduced blood flow (Y. Li et al., 2018). As a result, diminished perfusion into WM tissues is expected in healthy aging, and are suggested to underlie microstructural changes (Bagi et al., 2018; Chen et al., 2013). The results (**Figure 6**) of our cross-correlation analysis are key to the vascular hypothesis of WM aging, and indicate that age-related

deterioration may be detectable via ATT prior to most microstructural measures in certain tracts (particularly in the CST, SLFT, SLFP and UNC). Following this, AD_{perc} is the microstructural measure displaying detectable variations at the youngest ages. CBF_{perc} declines, in contrast, were detected at older ages than AD_{perc}. These lead us to hypothesize that ATT may be an earlier marker of WM decline than microstructure and WM CBF, to be confirmed in a longitudinal design. The superior sensitivity of vascular timing information to pathology would be consistent with recent reports on the unique sensitivity of vascular-response latency (Holmes et al., 2020; D. Kim et al., 2021; McKetton et al., 2019; Nanayakkara et al., 2023). In fact, ATT has previously been found to exhibit lower variability than CBF (Mutsaerts et al., 2015), which may underlie the finding that ATT, not CBF, displayed a detectable earlier variation in aging. Of the regions showing a leading variation in ATT_{perc} in the CCF analysis, the age associations with ATT_{perc} or any of the other parameters were not all particularly high or low, arguing against a detectability bias due to age effect size (**Figure 4**). The only tract in which ATT_{perc} variations lag those in microstructure is the ILF. As prior research has demonstrated an association between reduced perfusion in the cortex and the development of WM hyperintensities in related WM regions (Mayer et al., 2021), it is intuitive that changes in perfusion in the WM precede declines in WM integrity and ultimately the breakdown of WM tissue. This process likely results from the progressive inability of supporting glial cells to maintain myelin in WM fibers as perfusion (CBF) declines (Kobayashi et al., 2002; Kohama et al., 2012). Those axons with reduced or malformed myelin sheaths are then more vulnerable to age-related culling of vulnerable WM fibers, and associated WM regions at higher risk of pathological declines (Kohama et al., 2012; Tang et al., 1997). Related to cerebrovascular mapping, vascular response latency has been demonstrated as a more sensitive marker of pathology than response amplitude (Holmes et al., 2020; D. Kim et al., 2021; McKetton et al., 2019; Nanayakkara et al., 2023). Additionally, arterial-transit time (ATT) has been found to increase with advancing age (Mutsaerts et al., 2015). Moreover, arterial-transit time is reportedly independently related to white-matter lesions relative to CBF (Zhang et al., 2018). Thus, it is also interesting to determine whether CBF or ATT is an earlier marker of possible WM degeneration.

However, the ILF appears to be an exception in our results, in that all perfusion metrics lag microstructural ones. The ILF is characterized by a particularly low ATT_{perc}, but in general, we noted that the strength of the ATT_{perc} age effects is not associated with group-mean ATT_{perc} values, so the differences in the ATT's temporal evolutions across tracts remains unexplained. It is interesting to note that the ILF is the one most connected to the temporal cortex and temporal pole, among the earliest regions to deteriorate in aging (Cox et al., 2021), and a region with accelerated deterioration in cases of mild cognitive impairment and associated with early stages of Alzheimer's disease (X. Li et al., 2020; Wu et al., 2021). Thus, it is possible that the temporal brain tissue is differently susceptible to the aging process. More generally, glial function has been reported to deteriorate in aging independently of vascular factors (Angelova & Brown, 2019; Hanslik et al., 2021; Lau et al., 2023; Rawji et al., 2023). Clarifying peak-correlation shifted relationships in those tracts exhibiting linear declines will require either a wider age sample able to capture younger peak ATT values, or analysis of longitudinal data. A more comprehensive understanding of these differences would require accounting for physiological and developmental variation between tracts (REF paper 3). Nonetheless, this is the first time that WM perfusion has been directly demonstrated to vary at an earlier age than WM microstructure. We theorize that CBF and ATT reflect different aspects of vascular aging. However, vascular decline is fastest in the temporo-posterior tracts, while WM microstructural decline is fastest in the fronto-temporal tracts, suggesting vascular decline is not the sole contributor of WM decline. Future investigations should additionally consider the role of the anterior-posterior retrogenesis hypotheses (Hoagey et al., 2019; Raz, 2000; Slater et al., 2019).

4.1.5 Limitations

Our CCF analysis depends on nonlinearity in the age-associations of its inputs. While many tracts demonstrated significant quadratic declines, the heterogeneity of significant quadratic versus linear age effects restricted the tracts in which cross-measure tractwise comparisons could be conducted. Moreover, a notable limitation to these findings is that, while CBF_{perc} declined quadratically in all tracts but the

UNC, the predominantly linear declines in ATT_{perc} restricted the extent of possible timing comparisons. In any case, validating the temporal relationships and causal relationships will require the inclusion of longitudinal data.

One interesting possibility of WM perfusion findings in general is that different tracts, which may have become vascularized to different extents and at different developmental stages (Smirnov et al., 2021), may be differentially susceptible to degeneration. As cerebral microbleeds (CMB) are present in an estimated 23.5% of the healthy aging population (Litak et al., 2020; Pasi et al., 2017), rising from 17.8% in ages 60-69 to 38.3% over age 80 (Ding et al., 2015; Jeerakathil et al., 2004), there is little doubt that a degree of cerebral small vessel disease (CSVD) is present in this sample. The prevalence of these conditions in typical aging precludes their removal from a representative sample. CMB have been associated with a loss in general microstructural integrity consistent with the microstructure-microvascular associations indicated by this study (J.-Y. Liu et al., 2020), however, the local impact of possible lacunes on our sample is limited by TRACULA's deterministic probability tractography approach with anatomical priors (Maffei et al., 2021; Yendiki et al., 2011). Thus, for all practical purposes, tracts will not be interrupted even in the presence of CSVD. This was demonstrated in a recent paper by Maffei et al. (Maffei et al., 2023). Regardless, in future studies, we will also probe the effect of thresholding on segmentation and the differences between those with and without heavy CMB burden.

While evidence indicates the presence of notable impacts of menopause on WM integrity (Mosconi et al., 2021), self-report menopause status included in this data set was not sufficiently accurate to include in statistical analyses. Inclusion of more precise reporting of pre-, peri-, or post-menopausal status would be of considerable interest to furthering investigation of sex differences in WM aging. More generally, this study aimed to lay the groundwork for multimodal integration of aging metrics in the white matter and chose to address widely applied microstructural measures such as MD and FA. This introduces a number of limitations that may be resolved in more advanced diffusion modeling. This study also addressed only ten major WM tracts. These were chosen to minimize tract overlap/partial-voluming

between segmentations, however, additional comparisons may be possible in more recent segmentations (Maffei et al., 2021). Finally, while we have identified novel age-related findings using our paradigm, future exploration using longitudinal data would complement the cross-sectional nature of the HCP-A dataset used in this study.

4.2 Conclusions

Relationships between age, perfusion, and microstructural integrity assessed in this study depict highly tract-specific, as well as sex-specific, variation across our sample. The lack of a unified set of trends between perfusion and microstructural declines across tracts supports our hypothesis that WM perfusion and microstructure do not decline at the same rate in aging. Additionally, our secondary hypothesis that WM perfusion differences would be detectable earlier than differences in microstructural integrity, found support in that tractwise age effects on ATT_{perc} appear at earlier ages than multiple microstructural measures. Moreover, the ubiquity of CBF_{perc} as the chief driver of significant canonical perfusion-microstructure relationships demonstrates that CBF and ATT reflect different aspects of WM microvascular aging and should be investigated in more depth. To our knowledge, this study is the first demonstration of tractwise age effects in WM CBF and ATT, and these findings will be highly valuable to the development of a more complete model for mechanisms of brain aging.

Data Availability

Data analyzed in this study was drawn from the Human Connectome Project in Aging (HCP-A) (Bookheimer et al., 2019). All included HCP-A datasets were made available under appropriate data usage agreements and can be accessed via the NIMH Data Archive (https://nda.nih.gov/general-query.html?q=query=featured-datasets:Human%20Connectome%20Projects%20(HCP)).

Author Contributions

T. D. Robinson: Conceptualization, Methodology, Software, Formal Analysis, Data Curation, Writing - Original Draft, Visualization. **Y. L. Sun:** Software, Data Curation, Writing - Review & Editing. **P. T. H. Chang:** Software, Data Curation. **C. J. Gauthier:** Writing - Review & Editing. **J. J. Chen:** Conceptualization, Methodology, Formal Analysis, Writing - Review & Editing, Supervision, Project administration, Funding acquisition.

Declarations

Consent for Publication

All authors have consented to the publication of this study and its findings as an original research article in the journal GeroScience.

Declaration of Competing Interests

The authors have no conflicts of interest to declare, financial or otherwise, in the development or publication of this study.

Ethics Statement

All subject data included in this study was drawn from the Human Connectome Project In Aging (HCP-A) (Bookheimer et al., 2019). All subjects provided informed consent following assessment of their capability to provide said consent and these data were made available for use under appropriate data usage agreements.

Funding

This study was supported via grant funding from the Canadian Institutes of Health Research (CIHR) (#PJT169688), with additional financial support from the Canada Research Chairs (CRC) program, and the Vascular Training (VAST) Platform.

REFERENCES

Akashi, T., Takahashi, S., Mugikura, S., Sato, S., Murata, T., Umetsu, A., & Takase, K. (2017). Ischemic White Matter Lesions Associated With Medullary Arteries: Classification of MRI Findings Based on the Anatomic Arterial Distributions. *AJR. American Journal of Roentgenology*, *209*(3), W160–W168.

Alisch, J. S. R., Khattar, N., Kim, R. W., Cortina, L. E., Rejimon, A. C., Qian, W., Ferrucci, L., Resnick, S. M., Spencer, R. G., & Bouhrara, M. (2021). Sex and age-related differences in cerebral blood flow investigated using pseudo-continuous arterial spin labeling magnetic resonance imaging. *Aging*, *13*(4), 4911–4925.

Angelova, D. M., & Brown, D. R. (2019). Microglia and the aging brain: are senescent microglia the key to neurodegeneration? *Journal of Neurochemistry*, *151*(6), 676–688.

Bagi, Z., Brandner, D. D., Le, P., McNeal, D. W., Gong, X., Dou, H., Fulton, D. J., Beller, A., Ngyuen, T., Larson, E. B., Montine, T. J., Keene, C. D., & Back, S. A. (2018). Vasodilator dysfunction and oligodendrocyte dysmaturation in aging white matter. *Annals of Neurology*, *83*(1), 142–152.

Baker, L. M., Laidlaw, D. H., Conturo, T. E., Hogan, J., Zhao, Y., Luo, X., Correia, S., Cabeen, R., Lane, E. M., Heaps, J. M., Bolzenius, J., Salminen, L. E., Akbudak, E., McMichael, A. R., Usher, C., Behrman, A., & Paul, R. H. (2014). White matter changes with age utilizing quantitative diffusion MRI. *Neurology*, *83*(3), 247–252.

Bender, A. R., Völkle, M. C., & Raz, N. (2016). Differential aging of cerebral white matter in middle-aged and older adults: A seven-year follow-up. *NeuroImage*, *125*, 74–83.

Bernbaum, M., Menon, B. K., Fick, G., Smith, E. E., Goyal, M., Frayne, R., & Coutts, S. B. (2015). Reduced blood flow in normal white matter predicts development of leukoaraiosis. *Journal of Cerebral Blood Flow and Metabolism: Official Journal of the International Society of Cerebral Blood Flow and Metabolism*, *35*(10), 1610–1615.

Bookheimer, S. Y., Salat, D. H., Terpstra, M., Ances, B. M., Barch, D. M., Buckner, R. L., Burgess, G. C.,

Curtiss, S. W., Diaz-Santos, M., Elam, J. S., Fischl, B., Greve, D. N., Hagy, H. A., Harms, M. P., Hatch, O. M., Hedden, T., Hodge, C., Japardi, K. C., Kuhn, T. P., … Yacoub, E. (2019). The Lifespan Human Connectome Project in Aging: An overview. *NeuroImage*, *185*, 335–348.

Brickman, A. M., Meier, I. B., Korgaonkar, M. S., Provenzano, F. A., Grieve, S. M., Siedlecki, K. L., Wasserman, B. T., Williams, L. M., & Zimmerman, M. E. (2012). Testing the white matter retrogenesis hypothesis of cognitive aging. *Neurobiology of Aging*, *33*(8), 1699–1715.

Chen, J. J., Rosas, H. D., & Salat, D. H. (2011). Age-associated reductions in cerebral blood flow are independent from regional atrophy. *NeuroImage*, *55*(2), 468–478.

Chen, J. J., Rosas, H. D., & Salat, D. H. (2013). The relationship between cortical blood flow and sub-cortical white-matter health across the adult age span. *PloS One*, *8*(2), e56733.

Cox, S. R., Harris, M. A., Ritchie, S. J., Buchanan, C. R., Valdés Hernández, M. C., Corley, J., Taylor, A. M., Madole, J. W., Harris, S. E., Whalley, H. C., McIntosh, A. M., Russ, T. C., Bastin, M. E., Wardlaw, J. M., Deary, I. J., & Tucker-Drob, E. M. (2021). Three major dimensions of human brain cortical ageing in relation to cognitive decline across the eighth decade of life. *Molecular Psychiatry*, *26*(6), 2651–2662.

Damestani, N. L., Jacoby, J., Michel, C. B., Rashid, B., Salat, D. H., & Juttukonda, M. R. (2024). MRI assessment of cerebral white matter microvascular hemodynamics across the adult lifespan. *Journal of Magnetic Resonance Imaging*. https://doi.org/10.1002/jmri.29217

de Groot, M., Cremers, L. G. M., Ikram, M. A., Hofman, A., Krestin, G. P., van der Lugt, A., Niessen, W. J., & Vernooij, M. W. (2016). White Matter Degeneration with Aging: Longitudinal Diffusion MR Imaging Analysis. *Radiology*, *279*(2), 532–541.

de Groot, M., Ikram, M. A., Akoudad, S., Krestin, G. P., Hofman, A., van der Lugt, A., Niessen, W. J., & Vernooij, M. W. (2015). Tract-specific white matter degeneration in aging: the Rotterdam Study. *Alzheimer's & Dementia: The Journal of the Alzheimer's Association*, *11*(3), 321–330.

de la Torre, J. (2018). The Vascular Hypothesis of Alzheimer's Disease: A Key to Preclinical Prediction of Dementia Using Neuroimaging. *Journal of Alzheimer's Disease: JAD*, *63*(1), 35–52.

Difference of Median. (n.d.). Retrieved January 17, 2025, from https://www.itl.nist.gov/div898/software/dataplot/refman2/auxillar/diffmad.htm

Ding, J., Sigurdsson, S., Garcia, M., Phillips, C. L., Eiriksdottir, G., Gudnason, V., van Buchem, M. A., & Launer, L. J. (2015). Risk Factors Associated With Incident Cerebral Microbleeds According to Location in Older People: The Age, Gene/Environment Susceptibility (AGES)-Reykjavik Study. *JAMA Neurology*, *72*(6), 682–688.

Fan, Q., Nummenmaa, A., Witzel, T., Ohringer, N., Tian, Q., Setsompop, K., Klawiter, E. C., Rosen, B. R., Wald, L. L., & Huang, S. Y. (2020). Axon diameter index estimation independent of fiber orientation distribution using high-gradient diffusion MRI. *NeuroImage*, *222*, 117197.

Gast, H., Horowitz, A., Krupnik, R., Barazany, D., Lifshits, S., Ben-Amitay, S., & Assaf, Y. (2023). A Method for In-Vivo Mapping of Axonal Diameter Distributions in the Human Brain Using Diffusion-Based Axonal Spectrum Imaging (AxSI). *Neuroinformatics*, *21*(3), 469–482.

Giorgio, A., Santelli, L., Tomassini, V., Bosnell, R., Smith, S., De Stefano, N., & Johansen-Berg, H. (2010). Age-related changes in grey and white matter structure throughout adulthood. *NeuroImage*, *51*(3), 943–951.

Gold, E. B. (2011). The timing of the age at which natural menopause occurs. *Obstetrics and Gynecology Clinics of North America*, *38*(3), 425–440.

Hanslik, K. L., Marino, K. M., & Ulland, T. K. (2021). Modulation of glial function in health, aging, and neurodegenerative disease. *Frontiers in Cellular Neuroscience*, *15*. https://doi.org/10.3389/fncel.2021.718324

Harms, M. P., Somerville, L. H., Ances, B. M., Andersson, J., Barch, D. M., Bastiani, M., Bookheimer, S. Y., Brown, T. B., Buckner, R. L., Burgess, G. C., Coalson, T. S., Chappell, M. A., Dapretto, M., Douaud, G., Fischl, B., Glasser, M. F., Greve, D. N., Hodge, C., Jamison, K. W., … Yacoub, E. (2018). Extending the Human Connectome Project across ages: Imaging protocols for the Lifespan Development and Aging projects. *NeuroImage*, *183*, 972–984.

Harris, J. J., & Attwell, D. (2012). The energetics of CNS white matter. *The Journal of Neuroscience: The*

Official Journal of the Society for Neuroscience, *32*(1), 356–371.

Hase, Y., Horsburgh, K., Ihara, M., & Kalaria, R. N. (2018). White matter degeneration in vascular and other ageing-related dementias. *Journal of Neurochemistry*, *144*(5), 617–633.

Hoagey, D. A., Rieck, J. R., Rodrigue, K. M., & Kennedy, K. M. (2019). Joint contributions of cortical morphometry and white matter microstructure in healthy brain aging: A partial least squares correlation analysis. *Human Brain Mapping*, *40*(18), 5315–5329.

Holmes, K. R., Tang-Wai, D., Sam, K., McKetton, L., Poublanc, J., Crawley, A. P., Sobczyk, O., Cohn, M., Duffin, J., Tartaglia, M. C., Black, S. E., Fisher, J. A., Wasserman, B., & Mikulis, D. J. (2020). Slowed Temporal and Parietal Cerebrovascular Response in Patients with Alzheimer's Disease. *The Canadian Journal of Neurological Sciences. Le Journal Canadien Des Sciences Neurologiques*, *47*(3), 366–373.

Inano, S., Takao, H., Hayashi, N., Abe, O., & Ohtomo, K. (2011). Effects of age and gender on white matter integrity. *AJNR. American Journal of Neuroradiology*, *32*(11), 2103–2109.

Intzandt, B., Sanami, S., Huck, J., PREVENT-AD Research group, Villeneuve, S., Bherer, L., & Gauthier, C. J. (2023). Sex-specific relationships between obesity, physical activity, and gray and white matter volume in cognitively unimpaired older adults. *GeroScience*. https://doi.org/10.1007/s11357-023-00734-4

Jeerakathil, T., Wolf, P. A., Beiser, A., Hald, J. K., Au, R., Kase, C. S., Massaro, J. M., & DeCarli, C. (2004). Cerebral microbleeds: prevalence and associations with cardiovascular risk factors in the Framingham Study. *Stroke; a Journal of Cerebral Circulation*, *35*(8), 1831–1835.

Juttukonda, M. R., Li, B., Almaktoum, R., Stephens, K. A., Yochim, K. M., Yacoub, E., Buckner, R. L., & Salat, D. H. (2021). Characterizing cerebral hemodynamics across the adult lifespan with arterial spin labeling MRI data from the Human Connectome Project-Aging. *NeuroImage*, *230*, 117807.

Kandil, H., Soliman, A., Alghamdi, N. S., Jennings, J. R., & El-Baz, A. (2023). Using Mean Arterial Pressure in Hypertension Diagnosis versus Using Either Systolic or Diastolic Blood Pressure Measurements. *Biomedicines*, *11*(3). https://doi.org/10.3390/biomedicines11030849

Kim, C.-M., Alvarado, R. L., Stephens, K., Wey, H.-Y., Wang, D. J. J., Leritz, E. C., & Salat, D. H. (2020). Associations between cerebral blood flow and structural and functional brain imaging measures in individuals with neuropsychologically defined mild cognitive impairment. *Neurobiology of Aging*, *86*, 64–74.

Kim, D., Hughes, T. M., Lipford, M. E., Craft, S., Baker, L. D., Lockhart, S. N., Whitlow, C. T., Okonmah-Obazee, S. E., Hugenschmidt, C. E., Bobinski, M., & Jung, Y. (2021). Relationship Between Cerebrovascular Reactivity and Cognition Among People With Risk of Cognitive Decline. *Frontiers in Physiology*, *12*, 645342.

Kobayashi, K., Hayashi, M., Nakano, H., Fukutani, Y., Sasaki, K., Shimazaki, M., & Koshino, Y. (2002). Apoptosis of astrocytes with enhanced lysosomal activity and oligodendrocytes in white matter lesions in Alzheimer's disease. *Neuropathology and Applied Neurobiology*, *28*(3), 238–251.

Kohama, S. G., Rosene, D. L., & Sherman, L. S. (2012). Age-related changes in human and non-human primate white matter: from myelination disturbances to cognitive decline. *Age* , *34*(5), 1093–1110.

Kohn, J. C., Lampi, M. C., & Reinhart-King, C. A. (2015). Age-related vascular stiffening: causes and consequences. *Frontiers in Genetics*, *6*, 112.

Lau, V., Ramer, L., & Tremblay, M.-È. (2023). An aging, pathology burden, and glial senescence build-up hypothesis for late onset Alzheimer's disease. *Nature Communications*, *14*(1), 1670.

Lawrence, K. E., Nabulsi, L., Santhalingam, V., Abaryan, Z., Villalon-Reina, J. E., Nir, T. M., Ba Gari, I., Zhu, A. H., Haddad, E., Muir, A. M., Laltoo, E., Jahanshad, N., & Thompson, P. M. (2021). Age and sex effects on advanced white matter microstructure measures in 15,628 older adults: A UK biobank study. *Brain Imaging and Behavior*, *15*(6), 2813–2823.

Lee, J. (2022). Near-Lifespan Tracking of Cerebral Microvascular Degeneration in Aging to Alzheimer's Continuum. *Advances in Geriatric Medicine and Research*, *4*(1). https://doi.org/10.20900/agmr20220003

Liewald, D., Miller, R., Logothetis, N., Wagner, H.-J., & Schüz, A. (2014). Distribution of axon diameters in cortical white matter: an electron-microscopic study on three human brains and a macaque.

Biological Cybernetics, *108*(5), 541–557.

Litak, J., Mazurek, M., Kulesza, B., Szmygin, P., Litak, J., Kamieniak, P., & Grochowski, C. (2020). Cerebral Small Vessel Disease. *International Journal of Molecular Sciences*, *21*(24). https://doi.org/10.3390/ijms21249729

Liu, J.-Y., Zhou, Y.-J., Zhai, F.-F., Han, F., Zhou, L.-X., Ni, J., Yao, M., Zhang, S., Jin, Z., Cui, L., & Zhu, Y.-C. (2020). Cerebral Microbleeds Are Associated with Loss of White Matter Integrity. *AJNR. American Journal of Neuroradiology*, *41*(8), 1397–1404.

Liu, Y., Zhu, X., Feinberg, D., Guenther, M., Gregori, J., Weiner, M. W., & Schuff, N. (2012). Arterial spin labeling MRI study of age and gender effects on brain perfusion hemodynamics. *Magnetic Resonance in Medicine*, *68*(3), 912–922.

Li, X., Xia, J., Ma, C., Chen, K., Xu, K., Zhang, J., Chen, Y., Li, H., Wei, D., & Zhang, Z. (2020). Accelerating structural degeneration in temporal regions and their effects on cognition in aging of MCI patients. *Cerebral Cortex (New York, N.Y.: 1991)*, *30*(1), 326–338.

Li, Y., Choi, W. J., Wei, W., Song, S., Zhang, Q., Liu, J., & Wang, R. K. (2018). Aging-associated changes in cerebral vasculature and blood flow as determined by quantitative optical coherence tomography angiography. *Neurobiology of Aging*, *70*, 148–159.

Maffei, C., Gilmore, N., Snider, S. B., Foulkes, A. S., Bodien, Y. G., Yendiki, A., & Edlow, B. L. (2023). Automated detection of axonal damage along white matter tracts in acute severe traumatic brain injury. *NeuroImage. Clinical*, *37*, 103294.

Maffei, C., Lee, C., Planich, M., Ramprasad, M., Ravi, N., Trainor, D., Urban, Z., Kim, M., Jones, R. J., Henin, A., Hofmann, S. G., Pizzagalli, D. A., Auerbach, R. P., Gabrieli, J. D. E., Whitfield-Gabrieli, S., Greve, D. N., Haber, S. N., & Yendiki, A. (2021). Using diffusion MRI data acquired with ultra-high gradients to improve tractography in routine-quality data. In *bioRxiv* (p. 2021.06.28.450265). https://doi.org/10.1101/2021.06.28.450265

Mayer, C., Frey, B. M., Schlemm, E., Petersen, M., Engelke, K., Hanning, U., Jagodzinski, A., Borof, K., Fiehler, J., Gerloff, C., Thomalla, G., & Cheng, B. (2021). Linking cortical atrophy to white matter

hyperintensities of presumed vascular origin. *Journal of Cerebral Blood Flow and Metabolism: Official Journal of the International Society of Cerebral Blood Flow and Metabolism*, *41*(7), 1682–1691.

McKetton, L., Cohn, M., Tang-Wai, D. F., Sobczyk, O., Duffin, J., Holmes, K. R., Poublanc, J., Sam, K., Crawley, A. P., Venkatraghavan, L., Fisher, J. A., & Mikulis, D. J. (2019). Cerebrovascular Resistance in Healthy Aging and Mild Cognitive Impairment. *Frontiers in Aging Neuroscience*, *11*, 79.

Michielse, S., Coupland, N., Camicioli, R., Carter, R., Seres, P., Sabino, J., & Malykhin, N. (2010). Selective effects of aging on brain white matter microstructure: a diffusion tensor imaging tractography study. *NeuroImage*, *52*(4), 1190–1201.

Mosconi, L., Berti, V., Dyke, J., Schelbaum, E., Jett, S., Loughlin, L., Jang, G., Rahman, A., Hristov, H., Pahlajani, S., Andrews, R., Matthews, D., Etingin, O., Ganzer, C., de Leon, M., Isaacson, R., & Brinton, R. D. (2021). Menopause impacts human brain structure, connectivity, energy metabolism, and amyloid-beta deposition. *Scientific Reports*, *11*(1), 10867.

Mutsaerts, H. J. M. M., van Dalen, J. W., Heijtel, D. F. R., Groot, P. F. C., Majoie, C. B. L. M., Petersen, E. T., Richard, E., & Nederveen, A. J. (2015). Cerebral Perfusion Measurements in Elderly with Hypertension Using Arterial Spin Labeling. *PloS One*, *10*(8), e0133717.

Nanayakkara, N. D., Meusel, L.-A., Anderson, N. D., & Chen, J. J. (2023). Robust estimation of dynamic cerebrovascular reactivity using breath-holding fMRI: application in diabetes and hypertension. In *medRxiv*. https://doi.org/10.1101/2023.05.20.23290209

Nonaka, H., Akima, M., Hatori, T., Nagayama, T., Zhang, Z., & Ihara, F. (2003). Microvasculature of the human cerebral white matter: arteries of the deep white matter. *Neuropathology: Official Journal of the Japanese Society of Neuropathology*, *23*(2), 111–118.

Nozais, V., Forkel, S. J., Foulon, C., Petit, L., & Thiebaut de Schotten, M. (2021). Functionnectome as a framework to analyse the contribution of brain circuits to fMRI. *Communications Biology*, *4*(1), 1035.

O'Sullivan, M., Lythgoe, D. J., Pereira, A. C., Summers, P. E., Jarosz, J. M., Williams, S. C. R., & Markus, H. S. (2002). Patterns of cerebral blood flow reduction in patients with ischemic leukoaraiosis. *Neurology*, *59*(3), 321–326.

Pasi, M., Boulouis, G., Fotiadis, P., Auriel, E., Charidimou, A., Haley, K., Ayres, A., Schwab, K. M., Goldstein, J. N., Rosand, J., Viswanathan, A., Pantoni, L., Greenberg, S. M., & Gurol, M. E. (2017). Distribution of lacunes in cerebral amyloid angiopathy and hypertensive small vessel disease. *Neurology*, *88*(23), 2162–2168.

Patel, A., Chad, J. A., & Chen, J. J. (2023). Is adiposity associated with white matter microstructural health and intelligence differently in males and females? *Obesity* , *31*(4), 1011–1023.

Rawji, K. S., Neumann, B., & Franklin, R. J. M. (2023). Glial aging and its impact on central nervous system myelin regeneration. *Annals of the New York Academy of Sciences*, *1519*(1), 34–45.

Raz, N. (2000). Aging of the brain and its impact on cognitive performance: Integration of structural and functional findings. *The Handbook of Aging and Cognition., 2nd Ed.*, *2*, 1–90.

Robinson, T. D., Sun, Y. L., Chang, P. T. H., & Chen, J. J. (2024). Uncovering patterns of white matter degeneration in normal aging: Links between morphometry and microstructure. *Imaging Neuroscience*, *2*, 1–19.

Sala, S., Agosta, F., Pagani, E., Copetti, M., Comi, G., & Filippi, M. (2012). Microstructural changes and atrophy in brain white matter tracts with aging. *Neurobiology of Aging*, *33*(3), 488–498.e2.

Schilling, K. G., Archer, D., Yeh, F.-C., Rheault, F., Cai, L. Y., Hansen, C., Yang, Q., Ramdass, K., Shafer, A. T., Resnick, S. M., Pechman, K. R., Gifford, K. A., Hohman, T. J., Jefferson, A., Anderson, A. W., Kang, H., & Landman, B. A. (2022). Aging and white matter microstructure and macrostructure: a longitudinal multi-site diffusion MRI study of 1218 participants. *Brain Structure & Function*, *227*(6), 2111–2125.

Slater, D. A., Melie-Garcia, L., Preisig, M., Kherif, F., Lutti, A., & Draganski, B. (2019). Evolution of white matter tract microstructure across the life span. *Human Brain Mapping*, *40*(7), 2252–2268.

Smirnov, M., Destrieux, C., & Maldonado, I. L. (2021). Cerebral white matter vasculature: still

uncharted? *Brain: A Journal of Neurology*, *144*(12), 3561–3575.

Stricker, N. H., Schweinsburg, B. C., Delano-Wood, L., Wierenga, C. E., Bangen, K. J., Haaland, K. Y., Frank, L. R., Salmon, D. P., & Bondi, M. W. (2009). Decreased white matter integrity in late-myelinating fiber pathways in Alzheimer's disease supports retrogenesis. *NeuroImage*, *45*(1), 10–16.

Tang, Y., Nyengaard, J. R., Pakkenberg, B., & Gundersen, H. J. (1997). Age-induced white matter changes in the human brain: a stereological investigation. *Neurobiology of Aging*, *18*(6), 609–615.

Tomoto, T., Tarumi, T., & Zhang, R. (2023). Central arterial stiffness, brain white matter hyperintensity and total brain volume across the adult lifespan. *Journal of Hypertension*, *41*(5), 819–829.

Tosun, D., Mojabi, P., Weiner, M. W., & Schuff, N. (2010). Joint analysis of structural and perfusion MRI for cognitive assessment and classification of Alzheimer's disease and normal aging. *NeuroImage*, *52*(1), 186–197.

van Osch, M. J. P., Teeuwisse, W. M., van Walderveen, M. A. A., Hendrikse, J., Kies, D. A., & van Buchem, M. A. (2009). Can arterial spin labeling detect white matter perfusion signal? *Magnetic Resonance in Medicine: Official Journal of the Society of Magnetic Resonance in Medicine / Society of Magnetic Resonance in Medicine*, *62*(1), 165–173.

Vik, A., Hodneland, E., Haász, J., Ystad, M., Lundervold, A. J., & Lundervold, A. (2015). Fractional anisotropy shows differential reduction in frontal-subcortical fiber bundles—A longitudinal MRI study of 76 middle-aged and older adults. *Frontiers in Aging Neuroscience*, *7*. https://doi.org/10.3389/fnagi.2015.00081

Wang, D. J. J., Alger, J. R., Qiao, J. X., Gunther, M., Pope, W. B., Saver, J. L., Salamon, N., Liebeskind, D. S., & UCLA Stroke Investigators. (2013). Multi-delay multi-parametric arterial spin-labeled perfusion MRI in acute ischemic stroke - Comparison with dynamic susceptibility contrast enhanced perfusion imaging. *NeuroImage. Clinical*, *3*, 1–7.

Wierenga, C. E., Hays, C. C., & Zlatar, Z. Z. (2014). Cerebral blood flow measured by arterial spin labeling MRI as a preclinical marker of Alzheimer's disease. *Journal of Alzheimer's Disease: JAD*,

42 Suppl 4(Suppl 4), S411–S419.

Wu, B.-S., Zhang, Y.-R., Li, H.-Q., Kuo, K., Chen, S.-D., Dong, Q., Liu, Y., & Yu, J.-T. (2021). Cortical structure and the risk for Alzheimer's disease: a bidirectional Mendelian randomization study. *Translational Psychiatry*, *11*(1), 476.

Yeatman, J. D., Wandell, B. A., & Mezer, A. A. (2014). Lifespan maturation and degeneration of human brain white matter. *Nature Communications*, *5*, 4932.

Yendiki, A., Panneck, P., Srinivasan, P., Stevens, A., Zöllei, L., Augustinack, J., Wang, R., Salat, D., Ehrlich, S., Behrens, T., Jbabdi, S., Gollub, R., & Fischl, B. (2011). Automated probabilistic reconstruction of white-matter pathways in health and disease using an atlas of the underlying anatomy. *Frontiers in Neuroinformatics*, *5*, 23.

Zhang, N., Gordon, M. L., & Goldberg, T. E. (2017). Cerebral blood flow measured by arterial spin labeling MRI at resting state in normal aging and Alzheimer's disease. *Neuroscience and Biobehavioral Reviews*, *72*, 168–175.

Zhang, N., Gordon, M. L., Ma, Y., Chi, B., Gomar, J. J., Peng, S., Kingsley, P. B., Eidelberg, D., & Goldberg, T. E. (2018). The Age-Related Perfusion Pattern Measured With Arterial Spin Labeling MRI in Healthy Subjects. *Frontiers in Aging Neuroscience*, *10*, 214.

Zlokovic, B. V. (2011). Neurovascular pathways to neurodegeneration in Alzheimer's disease and other disorders. *Nature Reviews. Neuroscience*, *12*(12), 723–738.

Supplementary Materials

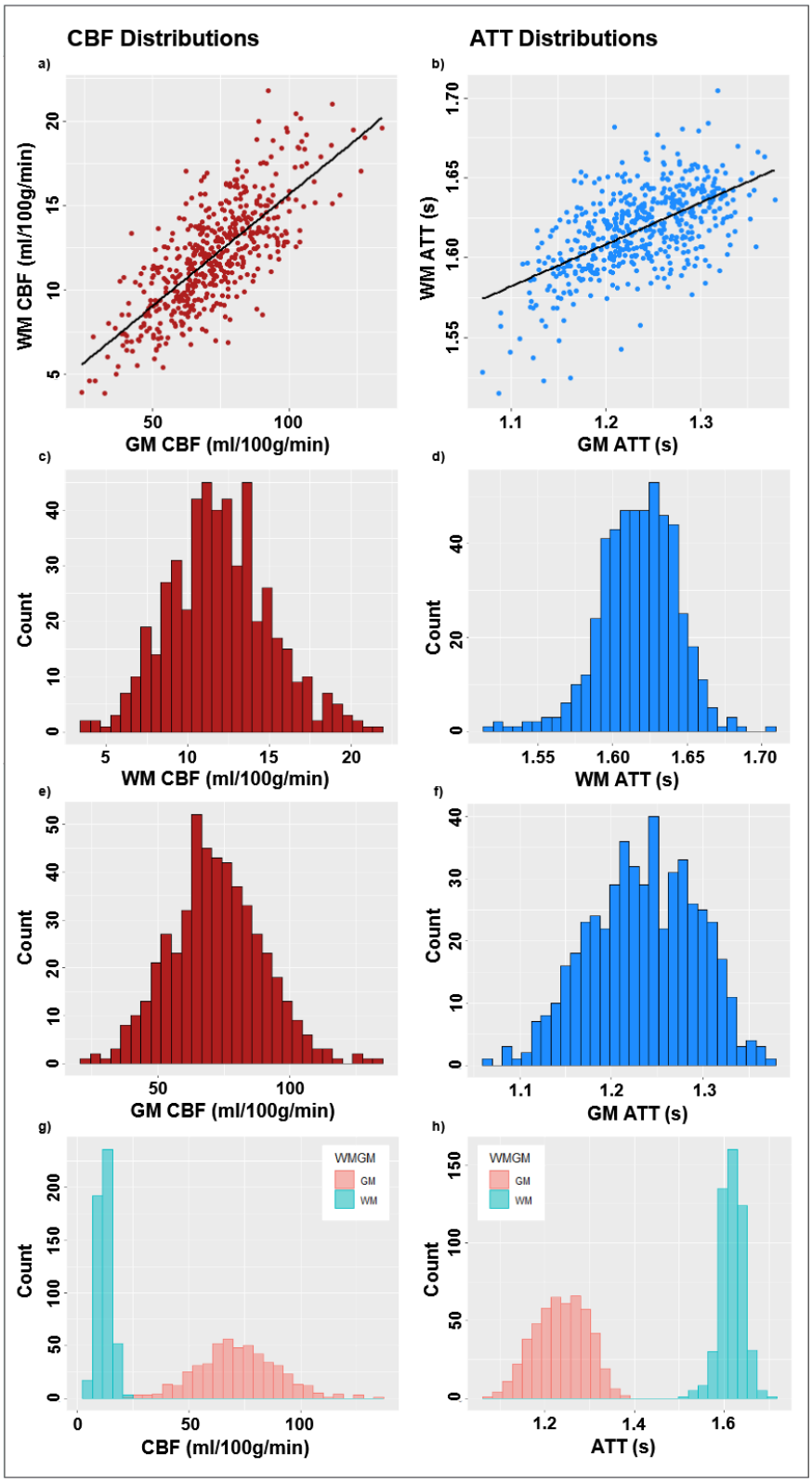

Supplementary Figure 1*: CBF and ATT distributions displayed between WM and GM values per subject (a, b), as separate counts for WM (c, d) and GM (e, f) across WM/GM specific ranges, and combined counts for both WM and GM values across the full CBF/ATT range within the sample (g, h)*

Supplementary Table 1a: Model 1 - Whole-WM MD/FA Relationships with Perfusion (Covaried for Sex).
All models are multivariate linear regressions based on baseline-normalized measures (x_{perc}) with overall F-statistics, *p*-values, and effect sizes ($R^2_{adjusted}$) listed. Slopes are noted below each regression equation and significant associations bolded with asterisks indicating significance. (*:p<.05, **:p<.01, ***:p<.001).

	MD_{perc}		**FA_{perc}**	
Tract	CBF_{perc}	ATT_{perc}	CBF_{perc}	ATT_{perc}
All	$F(2, 497) = 5.36$, $p = .005$, $R^2_{Adjusted} = .02$	$F(2, 497) = 4.07$, $p = .02$, $R^2_{Adjusted} = .01$	$F(2, 497) = 0.40$, $p = .67$, $R^2_{Adjusted} = -.002$	$F(2, 497) = 0.02$, $p = .98$, $R^2_{Adjusted} = -.004$
	-0.018508**	**0.231872***	0.0089404	0.0060844

Supplementary Table 1b: Model 1 - Tractwise MD/FA Relationships with Perfusion (Covaried for Sex).
All models are multivariate linear regressions based on baseline-normalized measures (x_{perc}) with overall F-statistics, *p*-values, and effect sizes ($R^2_{adjusted}$) listed. Slopes are noted below each regression equation and significant associations bolded with asterisks indicating significance. (*:p<.05, **:p<.01, ***:p<.001).

	MD_{perc}		**FA_{perc}**	
Tract	CBF_{perc}	ATT_{perc}	CBF_{perc}	ATT_{perc}
Fmajor	$F(2, 490) = 7.47$, $p < .001$, $R^2_{Adjusted} = .03$	$F(2, 490) = 5.68$, $p = .004$, $R^2_{Adjusted} = .02$	$F(2, 490) = 8.24$, $p < .001$, $R^2_{Adjusted} = .03$	$F(2, 490) = 8.08$, $p < .001$, $R^2_{Adjusted} = .03$
	-0.009599	0.081493	-0.003605	-0.010087
Fminor	$F(2, 490) = 1.52$, $p = .22$, $R^2_{Adjusted} = .002$	$F(2, 490) = 6,48$, $p = .002$, $R^2_{Adjusted} = .02$	$F(2, 490) = 5.49$, $p = .004$, $R^2_{Adjusted} = .02$	$F(2, 490) = 5.53$, $p = .004$, $R^2_{Adjusted} = .02$
	-0.011735	**0.289540****	0.019804	-0.227797
ATR	$F(2, 494) = 2.08$, $p = .13$, $R^2_{Adjusted} = .004$	$F(2, 494) = 9.13$, $p < .001$, $R^2_{Adjusted} = .03$	$F(2, 494) = 3.23$, $p = .009$, $R^2_{Adjusted} = .04$	$F(2, 494) = 4.22$, $p = .015$, $R^2_{Adjusted} = .01$
	-0.014611	**0.324941*****	0.027963	**-0.306558****

CAB	$F(2, 487) = 0.47$, $p = .62$, $R^2_{Adjusted} = -.002$	$F(2, 487) = 2.69$, $p = .07$, $R^2_{Adjusted} = .007$	$F(2, 487) = 0.75$, $p = .47$, $R^2_{Adjusted} = -.001$	$F(2, 487) = 4.53$, $p = .01$, $R^2_{Adjusted} = .01$
	0.0006211	-0.202510	0.01026	**0.79903***
CCG	$F(2, 492) = 2.48$, $p = .085$, $R^2_{Adjusted} = .006$	$F(2, 492) = 4.82$, $p = .008$, $R^2_{Adjusted} = .02$	$F(2, 492) = 13.3$, $p < .001$, $R^2_{Adjusted} = .05$	$F(2, 492) = 2.60$, $p = .006$, $R^2_{Adjusted} = .08$
	-0.013649	**0.216401****	**0.068524*****	0.050215
CST	$F(2, 488) = 6.42$, $p = .002$, $R^2_{Adjusted} = .02$	$F(2, 488) = 6.19$, $p = .002$, $R^2_{Adjusted} = .02$	$F(2, 488) = 1.89$, $p = .15$, $R^2_{Adjusted} = .004$	$F(2, 488) = 1.80$, $p = .17$, $R^2_{Adjusted} = .003$
	-0.006782	0.050971	-0.018407	0.225689
ILF	$F(2, 494) = 8.03$, $p < .001$, $R^2_{Adjusted} = .03$	$F(2, 494) = 3.67$, $p = .026$, $R^2_{Adjusted} = .01$	$F(2, 494) = 2.28$, $p = .10$, $R^2_{Adjusted} = .005$	$F(2, 494) = 2.90$, $p = .06$, $R^2_{Adjusted} = .008$
	-0.019481*	-0.032828	0.004481	0.16351
SLFP	$F(2, 494) = 3.64$, $p = .027$, $R^2_{Adjusted} = .01$	$F(2, 494) = 5.51$, $p = .004$, $R^2_{Adjusted} = .02$	$F(2, 494) = 2.15$, $p = .12$, $R^2_{Adjusted} = .005$	$F(2, 494) = 4.46$, $p = .012$, $R^2_{Adjusted} = .01$
	-0.014721	**0.214620***	-0.007393	-0.247955
SLFT	$F(2, 492) = 5.01$, $p = .007$, $R^2_{Adjusted} = .02$	$F(2, 492) = 7.78$, $p = .008$, $R^2_{Adjusted} = .02$	$F(2, 492) = 4.99$, $p = .007$, $R^2_{Adjusted} = .02$	$F(2, 492) = 3.37$, $p = .035$, $R^2_{Adjusted} = .009$
	-0.021370*	**0.222030***	-0.021391	-0.127256
UNC	$F(2, 492) = 0.49$, $p = .61$, $R^2_{Adjusted} = -.002$	$F(2, 492) = 0.82$, $p = .44$, $R^2_{Adjusted} = -.0007$	$F(2, 492) = 5.06$, $p = .007$, $R^2_{Adjusted} = .02$	$F(2, 492) = 4.33$, $p = .014$, $R^2_{Adjusted} = .01$
	-0.0055602	0.1058895	0.015398	-0.143507

Supplementary Table 2a: Model 2 - Whole-WM Sex Differences in Relationships Between MD/FA and Perfusion (Covaried for Age).
All models are multivariate linear regressions based on baseline-normalized measures (x_{perc}) with overall F-statistics, *p*-values, and effect sizes ($R^2_{adjusted}$) listed. Slopes are noted below each regression equation and significant associations bolded with asterisks indicating significance. (*:p<.05, **:p<.01, ***:p<.001).

	MD_{perc}				**FA_{perc}**			
	CBF_{perc}		ATT_{perc}		CBF		ATT	
Tract	Female	Male	Female	Male	Female	Male	Female	Male
All	$F(2, 291) = 55.5$, $p < .001$, $R^2_{Adjusted} = .27$	$F(2, 203) = 33.2$, $p < .001$, $R^2_{Adjusted} = .17$	$F(2, 291) = 55.1$, $p < .001$, $R^2_{Adjusted} = .27$	$F(2, 203) = 22.3$, $p < .001$, $R^2_{Adjusted} = .17$	$F(2, 291) = 9.72$, $p < .001$, $R^2_{Adjusted} = .06$	$F(2, 203) = 1.86$, $p = .16$, $R^2_{Adjusted} = .008$	$F(2, 291) = 9.51$, $p < .001$, $R^2_{Adjusted} = .05$	$F(2, 203) = 1.60$, $p = .20$, $R^2_{Adjusted} = .006$
	-0.0079527	-0.0007841	0.0559703	-0.0668848	0.0130418	-0.0143295	0.1261818	0.1857851

Supplementary Table 2b: Model 2 - Tractwise Sex Differences in Relationships Between MD/FA and Perfusion (Covaried for Age).
All models are multivariate linear regressions based on baseline-normalized measures (x_{perc}) with overall F-statistics, *p*-values, and effect sizes ($R^2_{adjusted}$) listed. Slopes are noted below each regression equation and significant associations bolded with asterisks indicating significance. (*:p<.05, **:p<.01, ***:p<.001).

	MD_{perc}				**FA_{perc}**			
	CBF_{perc}		ATT_{perc}		CBF_{perc}		$ATT_{percentage}$	
Tract	Female	Male	Female	Male	Female	Male	Female	Male
Fmajor	$F(2, 287) = 31.3$, $p < .001$, $R^2_{Adjusted} = .17$	$F(2, 200) = 9.30$, $p < .001$, $R^2_{Adjusted} = .009$	$F(2, 287) = 32.9$, $p < .001$, $R^2_{Adjusted} = .18$	$F(2, 200) = 8.95$, $p < .001$, $R^2_{Adjusted} = .07$	$F(2, 287) = 3.44$, $p = .034$, $R^2_{Adjusted} = .02$	$F(2, 200) = 1.96$, $p = .14$, $R^2_{Adjusted} = .009$	$F(2, 287) = 2.92$, $p = .056$, $R^2_{Adjusted} = .01$	$F(2, 200) = 1.96$, $p = .14$, $R^2_{Adjusted} = .009$
	-0.0039667	-0.0076777	0.1285074	0.0116263	-0.0093200	-0.0026277	-0.0444465	0.0518249

Fminor	$F(2, 288) = 77.5$, $p < .001$, $R^2_{Adjusted} = .35$	$F(2, 199) = 26.6$, $p < .001$, $R^2_{Adjusted} = .20$	$F(2, 288) = 76.8$, $p < .001$, $R^2_{Adjusted} = .34$	$F(2, 199) = 26.7$, $p < .001$, $R^2_{Adjusted} = .20$	$F(2, 288) = 24.4$, $p < .001$, $R^2_{Adjusted} = .14$	$F(2, 199) = 10.6$, $p < .001$, $R^2_{Adjusted} = .09$	$F(2, 288) = 22.0$, $p < .001$, $R^2_{Adjusted} = .13$	$F(2, 199) = 10.6$, $p < .001$, $R^2_{Adjusted} = .09$
	-0.0093523	-0.0011248	0.0490044	0.0443195	0.0248039	0.0045800	-0.0178029	-0.061765
ATR	$F(2, 289) = 63.6$, $p < .001$, $R^2_{Adjusted} = .30$	$F(2, 202) = 32.7$, $p < .001$, $R^2_{Adjusted} = .24$	$F(2, 289) = 65.0$, $p < .001$, $R^2_{Adjusted} = .31$	$F(2, 202) = 32.3$, $p < .001$, $R^2_{Adjusted} = .23$	$F(2, 289) = 8.25$, $p < .001$, $R^2_{Adjusted} = .05$	$F(2, 202) = 0.25$, $p = .78$, $R^2_{Adjusted} = -.007$	$F(2, 289) = 8.44$, $p < .001$, $R^2_{Adjusted} = .05$	$F(2, 202) = 0.08$, $p = .92$, $R^2_{Adjusted} = -.009$
	-0.0023397	-0.0075814	0.1296512	-0.0436909	**0.0427019***	0.0094317	**-0.3579011***	-0.0112258
CAB	$F(2, 285) = 14.5$, $p < .001$, $R^2_{Adjusted} = .09$	$F(2, 199) = 2.56$, $p = .08$, $R^2_{Adjusted} = .02$	$F(2, 285) = 14.3$, $p < .001$, $R^2_{Adjusted} = .08$	$F(2, 199) = 4.17$, $p = .016$, $R^2_{Adjusted} = .03$	$F(2, 285) = 7.74$, $p < .001$, $R^2_{Adjusted} = .04$	$F(2, 199) = 4.04$, $p = .02$, $R^2_{Adjusted} = .03$	$F(2, 285) = 11.2$, $p < .001$, $R^2_{Adjusted} = .07$	$F(2, 199) = 4.68$, $p = .01$, $R^2_{Adjusted} = .04$
	0.0114287	0.0064030	-0.1455464	-0.3302063	-0.0086050	-0.0161303	**0.7990257***	0.7374741
CCG	$F(2, 289) = 41.1$, $p < .001$, $R^2_{Adjusted} = .22$	$F(2, 200) = 18.6$, $p < .001$, $R^2_{Adjusted} = .15$	$F(2, 289) = 42.5$, $p < .001$, $R^2_{Adjusted} = .22$	$F(2, 200) = 18.4$, $p < .001$, $R^2_{Adjusted} = .15$	$F(2, 289) = 17.9$, $p < .001$, $R^2_{Adjusted} = .10$	$F(2, 200) = 11.5$, $p < .001$, $R^2_{Adjusted} = .09$	$F(2, 289) = 14.8$, $p < .001$, $R^2_{Adjusted} = .09$	$F(2, 200) = 6.26$, $p = .002$, $R^2_{Adjusted} = .05$
	-0.010615	-0.0046832	0.1605160	-0.0354249	**0.0482986***	**0.0755159*****	0.107982	0.5138831
CST	$F(2, 284) = 9.29$, $p < .001$, $R^2_{Adjusted} = .05$	$F(2, 201) = 1.37$, $p = .26$, $R^2_{Adjusted} = .004$	$F(2, 284) = 9.60$, $p < .001$, $R^2_{Adjusted} = .06$	$F(2, 201) = 1.35$, $p = .26$, $R^2_{Adjusted} = .003$	$F(2, 284) = 0.97$, $p = .38$, $R^2_{Adjusted} = -.0002$	$F(2, 201) = 3.67$, $p = .03$, $R^2_{Adjusted} = .03$	$F(2, 284) = 1.97$, $p = .14$, $R^2_{Adjusted} = .007$	$F(2, 201) = 1.29$, $p = .28$, $R^2_{Adjusted} = .003$
	0.0061903	-0.0065296	-0.1043070	0.0842141	-0.0054017	**-0.03705****	0.2295747	0.3193
ILF	$F(2, 289) = 43.0$, $p < .001$, $R^2_{Adjusted} = .22$	$F(2, 202) = 17.7$, $p < .001$, $R^2_{Adjusted} = .14$	$F(2, 289) = 41.8$, $p < .001$, $R^2_{Adjusted} = .22$	$F(2, 202) = 17.7$, $p < .001$, $R^2_{Adjusted} = .14$	$F(2, 289) = 10.3$, $p < .001$, $R^2_{Adjusted} = .06$	$F(2, 202) = 3.82$, $p = .02$, $R^2_{Adjusted} = .03$	$F(2, 289) = 10.7$, $p < .001$, $R^2_{Adjusted} = .06$	$F(2, 202) = 3.50$, $p = .03$, $R^2_{Adjusted} = .02$
	-0.0125893	0.0018092	0.0240348	0.0051664	-0.0020199	-0.0112217	0.1423583	0.0884416

SLFP	$F(2, 288) = 47.8$, $p < .001$, $R^2_{Adjusted} = .24$	$F(2, 203) = 20.6$, $p < .001$, $R^2_{Adjusted} = .16$	$F(2, 288) = 48.1$, $p < .001$, $R^2_{Adjusted} = .25$	$F(2, 203) = 20.8$, $p < .001$, $R^2_{Adjusted} = .16$	$F(2, 288) = 7.54$, $p < .001$, $R^2_{Adjusted} = .04$	$F(2, 203) = 1.73$, $p = .18$, $R^2_{Adjusted} = .007$	$F(2, 288) = 8,76$, $p < .001$, $R^2_{Adjusted} = .05$	$F(2, 203) = 0.41$, $p = .67$, $R^2_{Adjusted} = -.006$
	-0.0059281	0.0023829	0.0836243	0.0632643	-0.00005828	-0.02840	-0.2094319	-0.1595419
SLFT	$F(2, 287) = 52.9$, $p < .001$, $R^2_{Adjusted} = .26$	$F(2, 202) = 22.2$, $p < .001$, $R^2_{Adjusted} = .17$	$F(2, 287) = 53.6$, $p < .001$, $R^2_{Adjusted} = .27$	$F(2, 202) = 22.3$, $p < .001$, $R^2_{Adjusted} = .17$	$F(2, 287) = 4.30$, $p = .014$, $R^2_{Adjusted} = .02$	$F(2, 202) = 6.02$, $p = .003$, $R^2_{Adjusted} = .05$	$F(2, 287) = 4.59$, $p = .011$, $R^2_{Adjusted} = .02$	$F(2, 202) = 1.80$, $p = .17$, $R^2_{Adjusted} = .008$
	-0.0078787	0.0006048	0.1188965	0.0478854	-0.0097048	**-0.0440165****	-0.1308776	-0.0510914
UNC	$F(2, 290) = 49.5$, $p < .001$, $R^2_{Adjusted} = .25$	$F(2, 199) = 18.4$, $p < .001$, $R^2_{Adjusted} = .15$	$F(2, 290) = 49.8$ $p < .001$, $R^2_{Adjusted} = .25$	$F(2, 199) = 18.4$, $p < .001$, $R^2_{Adjusted} = .15$	$F(2, 290) = 3.21$, $p = .04$, $R^2_{Adjusted} = .01$	$F(2, 199) = 0.30$, $p = .74$, $R^2_{Adjusted} = -.007$	$F(2, 290) = 1.28$, $p = .28$, $R^2_{Adjusted} = .002$	$F(2, 199) = 0.32$, $p = .73$, $R^2_{Adjusted} = -.007$
	0.00004331	0.0009167	0.0632672	-0.0315701	0.0289662	-0.0053114	-0.1422849	-0.0935715